





ARTICLE

# Mitochondrial DNA segregation and replication restrict the transmission of detrimental mutation

Zhe Chen<sup>1\*</sup>, Zong-Heng Wang<sup>1\*</sup>, Guofeng Zhang<sup>2</sup>, Christopher K.E. Bleck<sup>1</sup>, Dillon J. Chung<sup>1</sup>, Grey P. Madison<sup>1</sup>, Eric Lindberg<sup>1</sup>, Christian Combs<sup>1</sup>, Robert S. Balaban<sup>1</sup>, and Hong Xu<sup>1</sup>

**Although mitochondrial DNA (mtDNA) is prone to accumulate mutations and lacks conventional DNA repair mechanisms, deleterious mutations are exceedingly rare. How the transmission of detrimental mtDNA mutations is restricted through the maternal lineage is debated. Here, we demonstrate that mitochondrial fission, together with the lack of mtDNA replication, segregate mtDNA into individual organelles in the *Drosophila* early germarium. After mtDNA segregation, mtDNA transcription begins, which activates respiration. Mitochondria harboring wild-type genomes have functional electron transport chains and propagate more vigorously than mitochondria containing deleterious mutations in heteroplasmic cells. Therefore, mtDNA expression acts as a stress test for the integrity of mitochondrial genomes and sets the stage for replication competition. Our observations support selective inheritance at the organelle level through a series of developmentally orchestrated mitochondrial processes. We also show that the Balbiani body has a minor role in mtDNA selective inheritance by supplying healthy mitochondria to the pole plasm. These two mechanisms may act synergistically to secure the transmission of functional mtDNA through *Drosophila* oogenesis.**

## Introduction

Mitochondria, the indispensable power plants of eukaryotic cells, present geneticists with a fundamental paradox. Their genome accumulates mutations at a high rate in the soma, estimated to be two orders of magnitude higher than that of the nuclear genome (Wallace and Chalkia, 2013). This rate owes to both the abundance of highly mutagenic free radicals generated by respiration and the lack of effective DNA repair via homologous recombination in the mitochondrial matrix (Taylor and Turnbull, 2005). If freely transmitted, the damaging mutations would gradually accumulate over generations, which could severely impair the fitness of organisms and even lead to their extinction (Felsenstein, 1974). However, damaging mitochondrial DNA (mtDNA) mutations are exceedingly rare in populations. This paradox underscores the existence of effective mechanisms that restrict the transmission of deleterious mtDNA mutations and favor the selective inheritance of healthy mitochondrial genomes. Because mtDNA is predominantly transmitted through the maternal lineage, these mechanisms must operate in the female germline.

Currently the dominant dogma, bottleneck inheritance, proposes that only a small fraction of the mitochondrial genomes

in a primordial germ cell (PGC) are transmitted to an oocyte and are eventually populated in the offspring. This process explains the rapid genetic drift of mitochondrial genotypes between generations (Hauswirth and Laipis, 1982; Olivo et al., 1983; Rebolledo-Jaramillo et al., 2014). Bottleneck inheritance could also indirectly lead to the counterselection of deleterious mtDNA mutations: different mtDNA compositions would generate different metabolic outputs in developing oocytes, eventually causing the elimination of oocytes harboring an excess of deleterious mutations (Jenuth et al., 1996). However, the frequency of spontaneous mtDNA mutations is  $\sim 10^{-5}$ – $10^{-6}$  (Cree et al., 2008), which, while high compared with the frequency of nuclear DNA mutations, remains too low to elicit the kind of biochemical deficiency required for an effective selection at the whole-cell level. In fact, deleterious mtDNA mutations are prevented from passing to the next generation even when present in low frequency in mouse models (Fan et al., 2008; Stewart et al., 2008b), underscoring the existence of a selection that likely occurs at the level of the individual organelle or genome.

Our work in *Drosophila melanogaster* (*Dm*) has shown that selective inheritance of mtDNA also takes place in insects (Hill

<sup>1</sup>National Heart, Lung, and Blood Institute, National Institutes of Health, Bethesda, MD; <sup>2</sup>National Institute of Biomedical Imaging and Bioengineering, National Institutes of Health, Bethesda, MD.

\*Z. Chen and Z-H. Wang contributed equally to this work; Correspondence to Hong Xu: [hong.xu@nih.gov](mailto:hong.xu@nih.gov); Zhe Chen: [zhe.chen@nih.gov](mailto:zhe.chen@nih.gov).

This is a work of the U.S. Government and is not subject to copyright protection in the United States. Foreign copyrights may apply. This article is distributed under the terms of an Attribution–Noncommercial–Share Alike–No Mirror Sites license for the first six months after the publication date (see <http://www.rupress.org/terms/>). After six months it is available under a Creative Commons License (Attribution–Noncommercial–Share Alike 4.0 International license, as described at <https://creativecommons.org/licenses/by-nc-sa/4.0/>).

et al., 2014). Taking advantage of a temperature-sensitive deleterious mtDNA mutation (*mt:Col<sup>T300I</sup>*, referred to as *ts*) that we had previously engineered (Hill et al., 2014), we found that the load of *ts* allele in the progeny of heteroplasmic mothers (carrying both wild-type and *ts* mtDNA) was greatly reduced at restrictive temperature (Hill et al., 2014). This observation suggests that the *Dm* female germline could detect the defect caused by the *ts* allele at restrictive temperature and limit its transmission. Genetic and developmental analyses roughly mapped selective mtDNA inheritance in *Dm* to a developmental window spanning the late germarium (region 2B) and early stages of egg chamber (Hill et al., 2014; Ma et al., 2014). This is the stage in which a group of 16 sister cells (16-cell cysts), derived from four successive divisions of a single cystoblast, organize into an egg chamber, from which a single egg will emerge (Spradling, 1993). Interestingly, this is also the stage when mtDNA replication resumes, after having been largely quiescent in dividing cysts and region 2A (Hill et al., 2014). mtDNA replication in this region appears to depend on active mitochondrial respiration, as both pharmacological inhibition and genetic disruption of nuclear-encoded electron-transport chain (ETC) subunits severely impair mtDNA replication (Hill et al., 2014). The *ts* mutation, which disrupts a subunit of the mitochondria-encoded ETC complex IV, greatly diminishes mtDNA replication in homoplasmic germaria at restrictive temperature (Hill et al., 2014). We proposed that in heteroplasmic germ cells, healthy mitochondria carrying wild-type mtDNA would replicate their DNA and propagate much more vigorously than defective ones harboring mutations that impair respiration. The replication-competition would consequently reduce the proportion of mutant mtDNA in progeny (Hill et al., 2014).

While logically compelling, the replication-competition model rests on the assumption that germ cells can discern the integrity of individual mitochondrial genomes, presumably based on their functionally distinct protein products. However, mitochondria are not stationary: they undergo constant fusion and fission, which mix and reassort mitochondrial genomes and their products (Frank et al., 2001; Ishihara et al., 2006; Legros et al., 2004). In heteroplasmic cells, mitochondrial fusion allows mtDNA complementation to maintain the overall metabolic output in spite of significant levels of mtDNA mutations (Chan, 2006). This process could therefore mask the functional deficiency caused by deleterious mutations and shield them from quality control processes. We hypothesize that mitochondrial genomes have to be effectively segregated and then expressed for replication-competition to be effective in selective mtDNA inheritance. However, currently, it is not clear whether and how mtDNA segregation and expression are regulated during oogenesis, nor do we know how such regulations impact mtDNA transmission and selective inheritance.

Aside from replication-competition and bottleneck inheritance, a mechanism has been proposed based on the observed localization and transport of mitochondria to the prospective germ plasm during oogenesis (Cox and Spradling, 2003). At the beginning of oocyte differentiation, a fraction of mitochondria and other organelles congregate to a structure called the Balbiani body, which supplies mitochondria to the pole plasm of mature

oocytes, the cytoplasm of the future embryos' PGCs. It has been proposed that healthy mitochondria might be enriched in the Balbiani body and preferentially transmitted to grandchildren (Cox and Spradling, 2003). However, the selective inheritance that we observed occurs in the immediate offspring of heteroplasmic mothers, arguing against that the Balbiani body plays a major role in this process. Nonetheless, it remains to be determined whether the Balbiani body may contribute to mtDNA selection by enriching healthy mitochondria in PGCs.

In this paper, we test the basic assumptions of our replication-competition model by documenting the behavior of mitochondria and their genomes in the *Dm* ovary. In addition, we examine the potential contribution of mitochondrial aggregation around the Balbiani body to selective mtDNA inheritance.

## Results

### Mitochondrial morphological change in *Dm* early germarium

Using optical microscopy, previous studies have demonstrated that mitochondria are more rounded and fragmented in dividing cysts compared with germline stem cells (GSCs) in *Dm* germarium region 1 (Cox and Spradling, 2003; Lieber et al., 2019), suggesting that mitochondria undergo increased fission or decreased fusion in germline cysts. To comprehensively analyze mitochondrial size and shape in germaria, we used focused ion beam scanning electron microscopy (FIB-SEM) to reconstruct a 3D volume of the *Dm* germarium at an isotropic resolution of  $10 \times 10 \times 10 \text{ nm}^3$  voxels (Videos 1 and 2). We then applied the computational segmentation to trace all mitochondria in germ cells. Overall, mitochondria displayed a wide spectrum of morphology, ranging from small spheres and short tubules to elongated tubules in germaria (Fig. 1, A and B). The mitochondrial volume appeared to be gradually decreased during cyst division (Fig. S1 A). In a two-cell cyst at region 1, 47.9% of the mitochondria were  $>0.05 \mu\text{m}^3$  (Fig. 1 E). After the completion of cyst division, the fraction of large mitochondria ( $>0.05 \mu\text{m}^3$ ) decreased to 18.8% in a 16-cell cyst at region 2A (Fig. 1 E). Reciprocally, the fraction of small mitochondria ( $<0.03 \mu\text{m}^3$ ) increased to 63.5%, compared with 37.5% in region 1 (Fig. 1 C and Table S1). We plotted the volume against the surface area of each individual mitochondrion to evaluate the geometric shape of mitochondria (Harris and Theriot, 2018). In region 1, two populations of mitochondria were observed (Fig. S1 B). One group of mitochondria were spherical, and the others were more elongated. In region 2A, more mitochondria shifted toward spheroid morphology (Fig. S1 C). These observations suggest that elongated, large mitochondria undergo fragmentation in dividing cysts in region 1 and become smaller spheroids in 16-cell cysts at region 2A.

To further substantiate this notion, we assessed mitochondrial morphology in germaria expressing dsRNA against *Fis1*, a mitochondrial outer membrane protein that promotes mitochondria fission (Stojanovski et al., 2004). *Fis1* RNAi was activated by a *bam-gal4* driver that expresses in dividing cysts specifically (Chen and McKearin, 2003; Fig. S2, A, B, and F). There were more large mitochondria ( $>0.05 \mu\text{m}^3$ ) and, correspondingly, fewer small mitochondria ( $0.01\text{--}0.03 \mu\text{m}^3$ ) in region

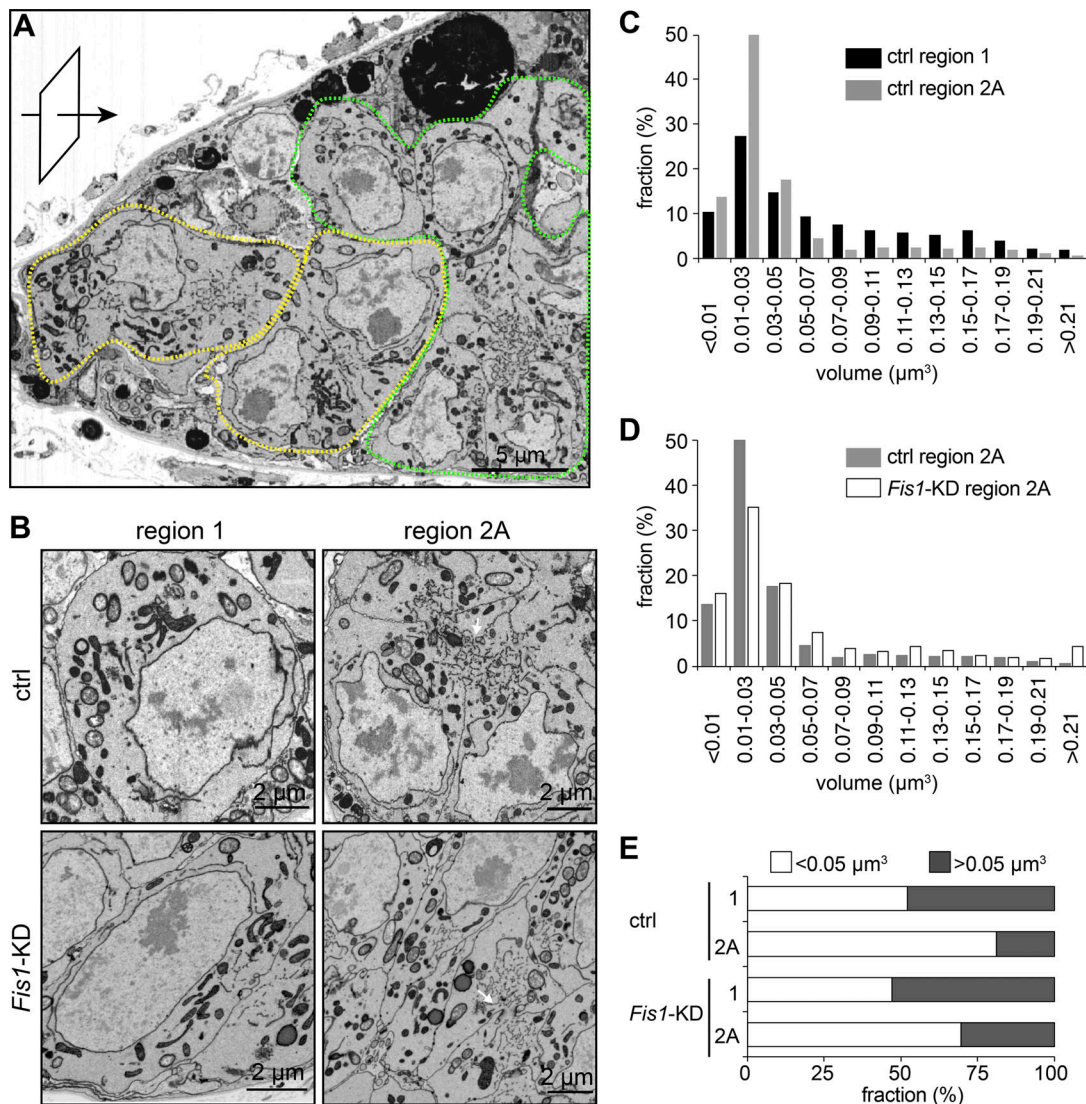


**Figure 1. Mitochondrial fragmentation in early germarium.** (A) A representative electron micrograph of wild-type early germarium obtained by FIB-SEM. Sample milling was performed from the anterior tip of the germarium toward the posterior (arrow). The image is a single section of xz plane after 3D reconstruction. Region 1 and region 2A cysts are outlined with yellow and green dashed lines, respectively. Scale bar, 5  $\mu\text{m}$ . (B) The detailed structures of mitochondria and other subcellular components in region 1 and region 2A of wild-type and *Fis1* knockdown by *bam-gal4*. The arrows point to ring canals between the germ cells and fusomes, which were used to trace the germ cells within a cyst. Scale bar, 2  $\mu\text{m}$ . (C and D) Frequency distribution of mitochondrial volume in region 1 ( $n = 808$  mitochondria) and region 2A ( $n = 4,782$  mitochondria) of wild-type germarium (C), and those in region 2A of wild-type and *Fis1* knockdown ( $n = 4,893$  mitochondria) germarium. (D) The proportion of mitochondria in the indicated range of volume. (E) The proportion of mitochondria with bigger ( $>0.05 \mu\text{m}^3$ ) volume from each experimental group (ctrl region 1,  $n = 808$ ; ctrl region 2A,  $n = 4,782$ ; *Fis1*-KD region 1,  $n = 510$ ; *Fis1*-KD region 2A,  $n = 4,893$ ).

2A compared with controls (Fig. 1 D), indicating that *Fis1* knockdown can effectively impede mitochondrial fragmentation in early germaria.

### Mitochondrial genomes are segregated in the region 2A germarium

We reasoned that the lack of mtDNA replication in region 2A (Hill et al., 2014), in conjunction with mitochondria fragmentation, would facilitate mitochondria genome segregation. To test this idea, we imaged the distribution of the mitochondrial genome in the mitochondrial network in germaria. Mitochondrial transcription factor A (TFAM) is the major mtDNA

packaging protein and a well-established marker for mtDNA nucleoids (Alam et al., 2003). We used stimulated emission depletion (STED) microscopy to image both the mitochondrial network and TFAM-GFP (Zhang et al., 2016) to assess mtDNA segregation (Fig. 2 A). Mitochondria labeled by ATP synthase  $\alpha$  subunit (ATPs) staining were more elongated and interconnected in GSCs or cystoblasts at region 1 and became more rounded in region 2A (Fig. 2, A and B). This result further substantiates that mitochondria undergo fragmentation in the early germarium as observed in the FIB-SEM analyses. The TFAM-GFP signal appeared as many puncta throughout the germarium and localized to mitochondria. We noticed that the



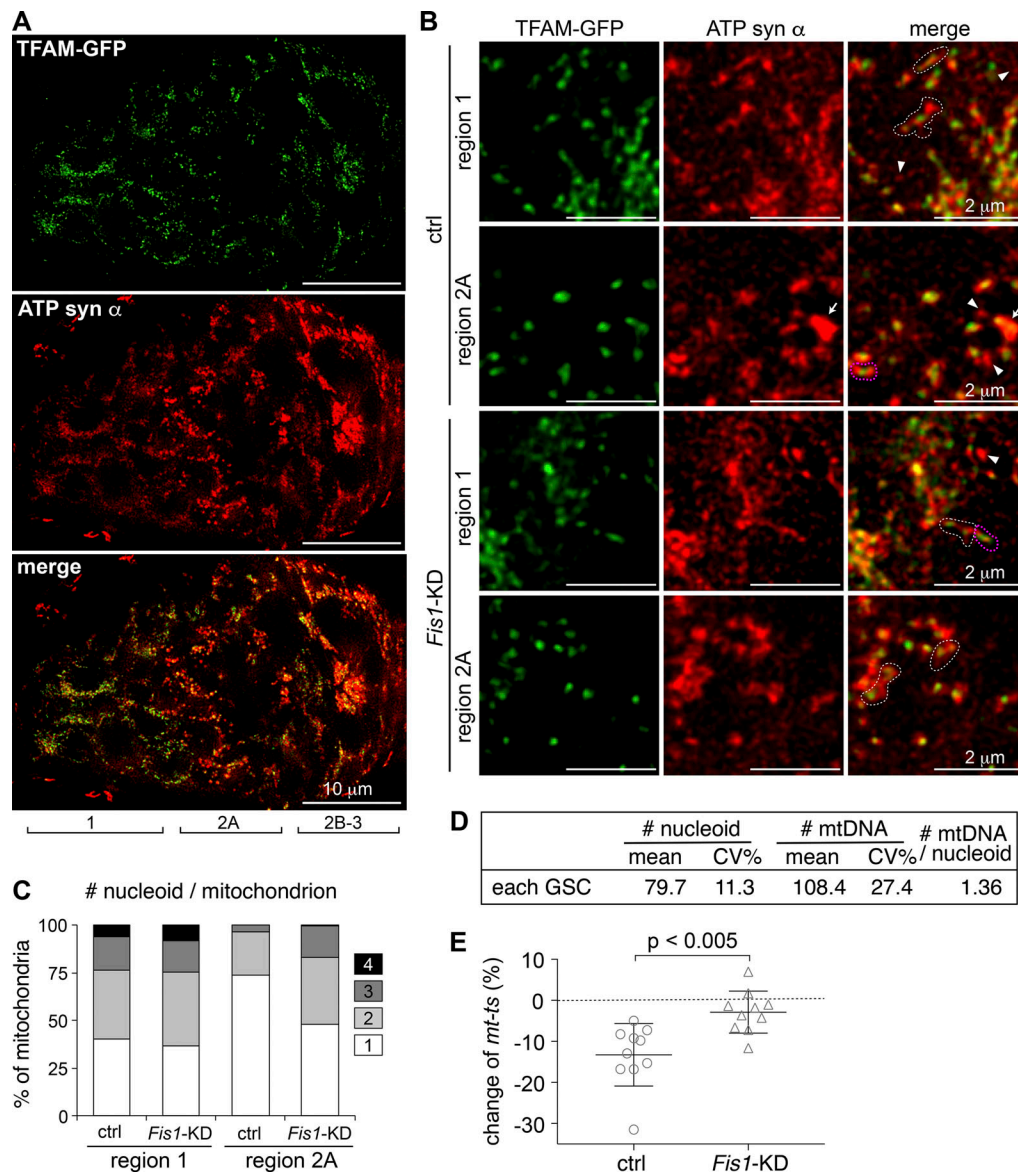


**Figure 2. Mitochondrial fragmentation and nucleoid segregation in gerarium region 2A are essential for mtDNA selective inheritance.** (A) Mitochondria labeled by ATPs staining and mtDNA labeled by TFAM-GFP in *Dm* gerarium. The images are representative z-stack projections (1.5  $\mu$ m) of a gerarium acquired with STED microscopy. The developmental regions of gerarium are indicated. Images are oriented with the gerarium anterior toward the left. Scale bar, 10  $\mu$ m. (B) Mitochondrial nucleoids labeled by TFAM-GFP and mitochondria labeled by ATPs staining in a gerarium are displayed in magnified views. Both control and *Fis1* knockdown ovaries driven by *bam-gal4* are shown. The representative images of region 1 are from the anterior end, where GSCs or cystoblasts reside. The white-dashed outlines are elongated mitochondria containing multiple nucleoids. Arrowheads point to mitochondria without nucleoids. The arrow points to clustered mitochondria, which are excluded from data analyses. The ATPs staining was uneven, with less intensity in the regions where nucleoids are located. We defined two adjacent but distinct ATPs puncta as a single mitochondrion if they appeared in the same contour and were connected to one nucleoid (magenta dashed outlines). Scale bar, 2  $\mu$ m. (C) The number of nucleoids per mitochondrion was determined using TFAM-GFP and ATPs staining shown in B in regions 1 (GSCs or cystoblasts) and 2A from control and *Fis1* knockdown ovaries ( $n = 5$  geraria for each genotype). The fraction of each group is shown. Note that the fraction of mitochondria containing multiple nucleoids was increased in region 2A of *Fis1* knockdown driven by *bam-gal4*. (D) Quantification of mitochondrial nucleoid number ( $n = 5$ ) and mtDNA copy number ( $n = 6$ ) in each germ stem cell (GSC) in gerarium. CV, coefficient of variance. (E) Knockdown of *Fis1* in gerarium region 2A, using a *bam-Gal4* driver, compromised the selection against the mutant mtDNA in heteroplasmic *mt:Col<sup>T300I</sup> Dm*. The proportion of mutant *ts* mtDNA in progeny was decreased by 15% compared with their mothers on average. In *Fis1* knockdown fly, this negative selection was diminished. Data presented are means  $\pm$  SD ( $n = 10$  for each genotype).  $P < 0.005$ .

ATPs staining was not always uniform along the mitochondrial network, which might reflect the uneven density of cristae, where the ATP synthase locates, in different mitochondria. Sometimes, even within a single mitochondrion, ATPs staining appeared as multiple puncta, and nucleoids were located in regions

with low ATPs intensity (Fig. 2 B). This phenomenon is in line with a recent superresolution microscopic study showing a lack of cristae structures surrounding nucleoids (Stephan et al., 2019).

We next quantified the number of nucleoids in each mitochondrion. In the anterior end of region 1, where GSCs and

cystoblasts reside, the number of mitochondrial nucleoids, indicated as the TFAM-GFP puncta, ranged from zero to four in different mitochondria (Fig. 2 C). As expected, large and elongated mitochondria often contained more than one nucleoid, whereas some small mitochondria, which might be the intermediate structures of mitochondrial fusion and fission processes, were devoid of TFAM-GFP signal (Fig. 2 B). Among TFAM-GFP-positive mitochondria, 40.4, 36, 17.4, and 6.2% of them contained one, two, three, and four nucleoids, respectively (Fig. 2 C). In region 2A, 73.9% of the mitochondria contained only one nucleoid (Fig. 2 C), indicating that through mitochondrial fragmentation, nucleoids are effectively segregated in 16-cell cysts at region 2A before the onset of mtDNA replication in germarium region 2B.

It has been estimated that a single nucleoid may contain 1–10 copies of mtDNA (Kukat et al., 2011; Legros et al., 2004; Satoh and Kuroiwa, 1991). Although mtDNA in separate nucleoids do not intermix (Gilkerson et al., 2008), those within a nucleoid can functionally complement each other, which could interfere with selective inheritance (Hill et al., 2014). Currently, there is no reliable technique to accurately quantify mtDNA copy number within a specific nucleoid. We considered using TFAM-GFP intensity as a measure for mtDNA copy number in a nucleoid; however, the values of TFAM-GFP intensity in different nucleoids appeared to be random and continuous, instead of quantized. It is known that TFAM-GFP intensity is affected by not only mtDNA copy number but also the compaction state of mtDNA in a nucleoid (Kukat et al., 2011). Nonetheless, one could approximate mtDNA copy number per nucleoid by normalizing the total number of mitochondrial genomes to the number of nucleoids in a cell. To this end, we isolated germ cells by FACS from white pupae expressing Vasa-GFP, a reporter specific to germ cells (Fig. S3 A). At this stage, oogenesis has progressed to the region 1 germarium, which consists mainly of GSCs and cystoblasts (Song et al., 2007). We quantified the mtDNA copy number to be ~108 copies in GSCs and early cysts (Fig. 2 D). We also quantified the mtDNA copy number in a female germline stem cell (fGS) culture established from *Dm* adult ovaries (Niki et al., 2006). We estimated there were ~120 copies of mtDNA per fGS cell (Fig. S3 B), which is close to the value obtained from germ cells in early pupae ovaries. Because there were ~80 nucleoids in GSCs (Fig. 2 D), we deduced that each nucleoid contained 1.36 copies of mtDNA on average. This approximation suggests that intranucleoid complementation is rather minimal at this stage. In addition, given that there is no mtDNA replication until region 2B (Hill et al., 2014), the mtDNA copy number within a nucleoid should not increase before the stage when selective inheritance occurs. Taken together, our observations indicate that mtDNA molecules are effectively sorted into different organelles during the early stages of ovarian development.

#### Mitochondrial segregation is required for mtDNA selective inheritance

To test whether mtDNA segregation is required for selective inheritance, we attempted to increase the number of nucleoids per mitochondrion by tampering with mitochondrial fission. We quantified the number of nucleoids in individual mitochondria

in *Fis1* knockdown flies (Fig. 2, B and C). In 16-cell cyst region 2A, only 47.7% of mitochondria contained a single nucleoid, compared with 73.9% in wild type (Fig. 2 C). Additionally, RNAi against *Drp1* (Fig. S2, B and F; and Fig. S4, A and B), a large GTPase that promotes mitochondria fission (Labrousse et al., 1999), caused similar phenotypes as these in *Fis1* knockdown flies. Thus, inhibition of mitochondrial fission impairs mitochondria genome segregation.

We next tested the impact of impaired mitochondrial fragmentation on mtDNA selective inheritance in heteroplasmic flies. We knocked down *Fis1* or *Drp1* in the female germline of heteroplasmic flies using *bam-gal4* driver (Fig. S2 A, B, and F; and Fig. S5), and compared mutation loads in mothers and their eggs. Under the restrictive temperature, the average proportion of *ts* allele was decreased by 15% in eggs compared with their mothers in control flies (Fig. 2 E), indicating selection against the deleterious mtDNA. By contrast, in both *Fis1* RNAi and *Drp1* RNAi flies, the load of *ts* allele displayed a pattern of random mtDNA segregation, with no clear reduction in progeny (Figs. 2 E and S4 C). Taken together, these observations indicate that mitochondrial fission promotes nucleoid segregation in region 2A and is required for effective mtDNA selection.

#### Mitochondrial activity and mtDNA expression commence in region 2B

We hypothesized that ETC genes on mitochondrial genomes had to be expressed for heteroplasmic cells to distinguish different mtDNA genotypes. To test this idea, we examined the pattern of mtDNA-encoded gene expression in the germline by FISH, using short DNA probes targeted to two mtDNA-encoded mRNAs: *NADH dehydrogenase 4 (ND4)* and *cytochrome c oxidase subunit 1 (CoI)* (Fig. 3 A). For either *ND4* or *CoI*, a moderate level of mRNA was detected in the anterior end of region 1, but almost no signal in region 2A. In the following 16-cell cysts at region 2B, strong FISH signal was observed, suggesting that mtDNA expression commences at this stage (Fig. 3 B). We also examined the expression pattern of two ETC genes encoded in the nuclear genome: *NADH: ubiquinone oxidoreductase subunit B5 (NDUFB5)* and *cox5A* (Fig. 3 A). Both transcripts showed an expression pattern similar to that of mtDNA-encoded mRNAs, i.e., moderate expression in GSCs, nearly no expression in region 2A, and strong expression in region 2B (Fig. 3 B). Interestingly, the shape and the localization of these two transcripts resembled those of mitochondria at the region 2B germarium, which is consistent with previous studies that mitochondrial ETC genes undergo local translation on mitochondrial outer membrane (Williams et al., 2014; Zhang et al., 2016).

The coordinated expression of both mitochondrial and nuclear ETC genes in region 2B led us to ask whether mitochondrial respiration was also activated at this stage. To address this question, we analyzed mitochondrial membrane potential in germarium, using tetramethylrhodamine methyl ester (TMRM), a dye that preferentially accumulates in polarized mitochondria (Scaduto and Grotyohann, 1999). We found that the ratio of TMRM to MitoTracker green (a marker of mitochondrial mass) was markedly increased in germline region 2B compared with regions 1 and 2A (Fig. 3 C), indicating that mitochondrial

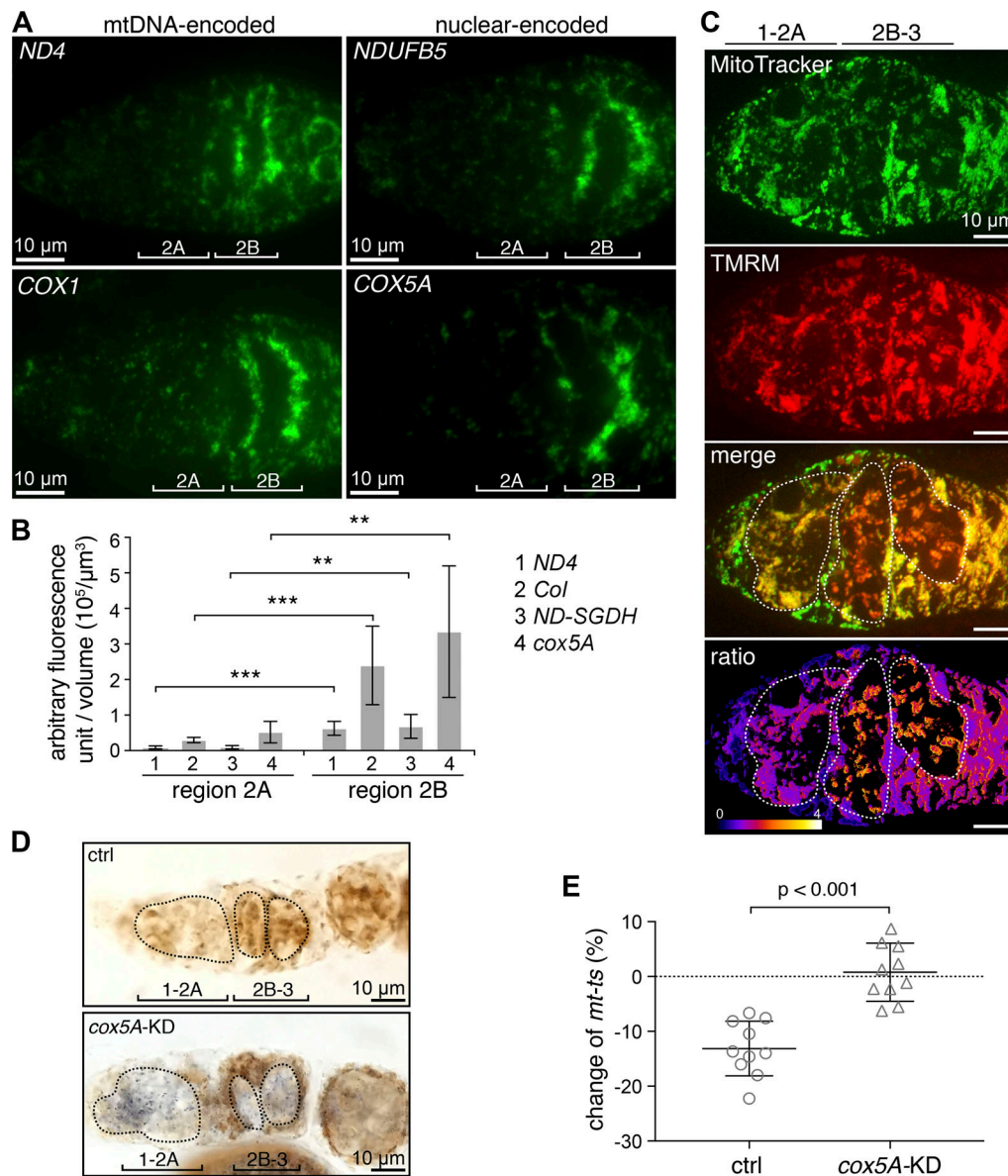


**Figure 3. Mitochondrial respiration is activated in region 2B and is essential for mtDNA selective inheritance. (A)** Expression of mtDNA- and nuclear-encoded ETCs genes in the germarium. The spatial patterns of nuclear and mitochondrial encoded mRNAs were revealed by smFISH assay. Fluorescently labeled probes targeted mtDNA-encoded *ND4* and *Col* transcripts and the nuclear-encoded *ND-SGDH* and *cox5A* transcripts. Scale bar, 10  $\mu$ m. **(B)** Quantification of total immunofluorescence intensity per volume in regions 2A and 2B ( $n = 6$ ). The expression of all RNAs was markedly increased at region 2B. Data presented are means  $\pm$  SD. \*\*,  $P < 0.005$ ; \*\*\*,  $P < 0.001$ . **(C)** Mitochondria membrane potential staining demonstrated by the mitochondrial membrane potential indicator TMRM (red) and mitochondrial fluorescent dye MitoTracker (green). The strong red signal indicates markedly increased membrane potential at regions 2B and 3 in merged image. The ratio of red to green fluorescence intensity is shown as the pseudo-color ratiometric image. The developing regions of germarium germ cells are outlined. Scale bar, 10  $\mu$ m. **(D)** Mitochondrial respiratory activity in ovary using the colorimetric assay. Ovaries from control and *cox5A* knockdown flies driven by *nanos-gal4* were stained for dual succinate dehydrogenase (complex II) and cytochrome c oxidase (complex IV) activity. Representative images for each group are shown. Intense brown color, indicating that both complex II and complex IV are active, was prominent in region 2B but mostly absent in regions 1 and 2A. The blue color indicates that complex IV activity is greatly reduced in *cox5A* knockdown ovary. The developing regions of germarium germ cells are outlined. Scale bar, 10  $\mu$ m. **(E)** Selection against the deleterious mtDNA mutation (*ts*) in heteroplasmic flies was compromised by knocking down *cox5A* in the germline using *nanos-gal4* driver ( $n = 10$  for each genotype). Data presented are means  $\pm$  SD.  $P < 0.001$ .

membrane potential is low in early stage cysts but up-regulated at region 2B. The low level of membrane potential in the early germarium might be caused simply by a lack of ETCs. To assess the level of ETCs, we directly evaluated activities of ETCs in a colorimetric assay by incubating ovaries with substrates of succinate dehydrogenase (complex II) and cytochrome c oxidase

(complex IV). Intense brown color, indicating that both complex II and complex IV are active (Ross, 2011), was evident in region 2B, but mostly absent in region 1 and region 2A (Fig. 3 D). This result is consistent with the mitochondrial membrane potential staining (Fig. 3 C), indicating that mitochondrial respiration is low in early germarium but elevated in region 2B. Given their



co-occurrence, the elevation of respiration could be at least partially due to the onset of mtDNA expression that generates ETCs in differentiating cysts region 2B.

### Mitochondrial activation in late germarium stage allows the selective propagation of functional mtDNA

Based on the results above, we hypothesized that mtDNA expression and the following activation of respiration may act as a stress test allowing germ cells to distinguish between mitochondria that harbor wild-type versus a mutant mtDNA. We hence predicted that a ubiquitous disruption of mitochondrial activity in a heteroplasmic germ cell would mask the deficiency of mitochondria harboring the deleterious mtDNA mutation and impair selective inheritance. To ubiquitously disrupt respiration in all mitochondria, we knocked down a nuclear-encoded ETC gene, *cox5A*, in ovaries driven by *nanos-gal4* (Fig. S2 A). Strong knockdown of *cox5A* led to degeneration of ovaries. We were able to find an appropriate RNAi line that moderately decreased the mRNA level of *cox5A* (Fig. S2, D and F) but did not affect the fecundity of the female flies or the hatching rate of their progeny (Fig. S5). Nonetheless, complex IV activity was markedly decreased in the knockdown germarium (Fig. 3 D). Importantly, knockdown of *cox5A* in heteroplasmic *mt:Col<sup>T300I</sup>* background severely impaired selection against the *ts* allele (Fig. 3 E).

The universal disruption of mitochondrial respiration by knocking down *cox5A* in a germ cell not only masks the differential energetic status among different mitochondria, but also could impair cellular energy metabolism, which indirectly affects selective inheritance. If the activation of mitochondrial respiration in region 2B indeed functions as the stress test for mtDNA integrity, we anticipated that improving the respiratory activity of defective mitochondria carrying deleterious mutations would also weaken selective inheritance in heteroplasmic flies. We previously showed that the ectopic expression of an alternative oxidase, AOX, that catalyzes electron transfer from ubiquinone to molecular oxygen and bypasses the cytochrome chain reactions, completely restores the viability of *mt:Col<sup>T300I</sup>* flies (Chen et al., 2015). Expression of AOX in the germ cells driven by *nanos-gal4* partially restored mtDNA replication in region 2B of homoplasmic *ts* flies raised at 29°C (Fig. 4, A and C) but had no effect on female fecundity or embryo hatching rate (Fig. S5). Because mtDNA replication in region 2B depends on active respiration (Hill et al., 2014), this observation suggests that AOX overexpression rescues mitochondrial respiration of *ts* flies at restrictive temperature. Importantly, the reduction of *ts* allele was much less pronounced in progeny of AOX overexpression flies than controls (Fig. 4 D), indicating that mitigating the mitochondrial deficiency caused by *ts* mtDNA impairs the selection process.

The fact that improving respiration in heteroplasmic flies, without affecting the overall cellular energy metabolism, can weaken selective inheritance supports that germ cells indeed rely on the respiratory activity of individual mitochondria to gauge the integrity of the genome. Based on our replication-competition model, wild-type mtDNA harbored by healthy mitochondria would replicate more efficiently than mutant mtDNA in respiration-defective organelles. This model predicts that

mtDNA replication would be required for selective inheritance. To test this idea, we attempted to inhibit mtDNA replication in heteroplasmic flies. We found that knockdown of mitochondrial single-stranded DNA binding protein (*mtSSB*), an essential factor for mtDNA replication (Korhonen et al., 2004), markedly reduced mtDNA replication in region 2B (Fig. S2 E and Fig. 4, B and C), whereas mtDNA replication in later-stage egg chambers appeared unaffected (Fig. 4 B). This result is consistent with the notion that mtDNA replication in region 2B is particularly sensitive to mitochondrial disruption (Hill et al., 2014). Importantly, knockdown of *mtSSB* in heteroplasmic flies greatly diminished selective inheritance (Figs. 4 E and S5). Additionally, RNAi against *tamas*, the mtDNA polymerase, also diminished the selection against *ts* mtDNA (Figs. S4 D and S5), supporting that mtDNA replication in region 2B is indeed necessary for selective inheritance. Taken together, these results suggest that activation of mitochondrial respiration serves as a stress test to identify healthy mitochondria and promotes the replication of their mtDNA.

### The Balbiani body has a minor contribution to selective inheritance in germ cells

We have shown that mtDNA molecules are effectively segregated before region 2B and begin expressing their genes and replicating in region 2B. In a heteroplasmic background, these concerted processes presumably allow the healthy mitochondria containing wild-type mtDNA to outcompete the defective mitochondria harboring deleterious mutations in developing germ cells, which effectively reduces the proportion of mtDNA mutations in mature oocytes.

A model of developmentally regulated localization and transport of mitochondria has also been proposed to contribute to mtDNA selection (Cox and Spradling, 2003). In germarium region 2B, healthy mitochondria are preferentially associated with fusome (Hill et al., 2014). Some fusome-associated mitochondria will be transported to the Balbiani body and populate in the pole plasm (Cox and Spradling 2006), the cytoplasm of future PGCs. Thus, one would expect a lower level of mtDNA mutations in PGCs than somatic cells in an embryo. To test this idea, we isolated PGCs from fertilized eggs of heteroplasmic flies expressing a germ cell-specific reporter, Vasa-GFP, by fluorescence-based cell sorting and compared levels of the *ts* allele in PGCs and somatic cells. At 29°C, the proportion of *ts* genomes in PGCs was slightly, but consistently, lower than in somatic cells isolated from the same batch of embryos (Fig. 5 A). The difference in heteroplasmic level between PGCs and somatic tissues was ~3% on average. To confirm that this difference in fact results from an enrichment for healthy mitochondria in the Balbiani body, we performed the same experiment in the context of a germline-specific knockdown of *milton*, the adaptor that mediates the Kinesin-dependent transport of mitochondria to the Balbiani body (Cox and Spradling, 2006). In forming follicles, there were much fewer mitochondria at the anterior end of the *milton*-knockdown oocyte compared with the control (Fig. 5 B). Mitochondria dispersed throughout the cytoplasm of the oocyte in the control stage 5 egg chambers. However, *milton*-knockdown oocytes contained much fewer mitochondria, most

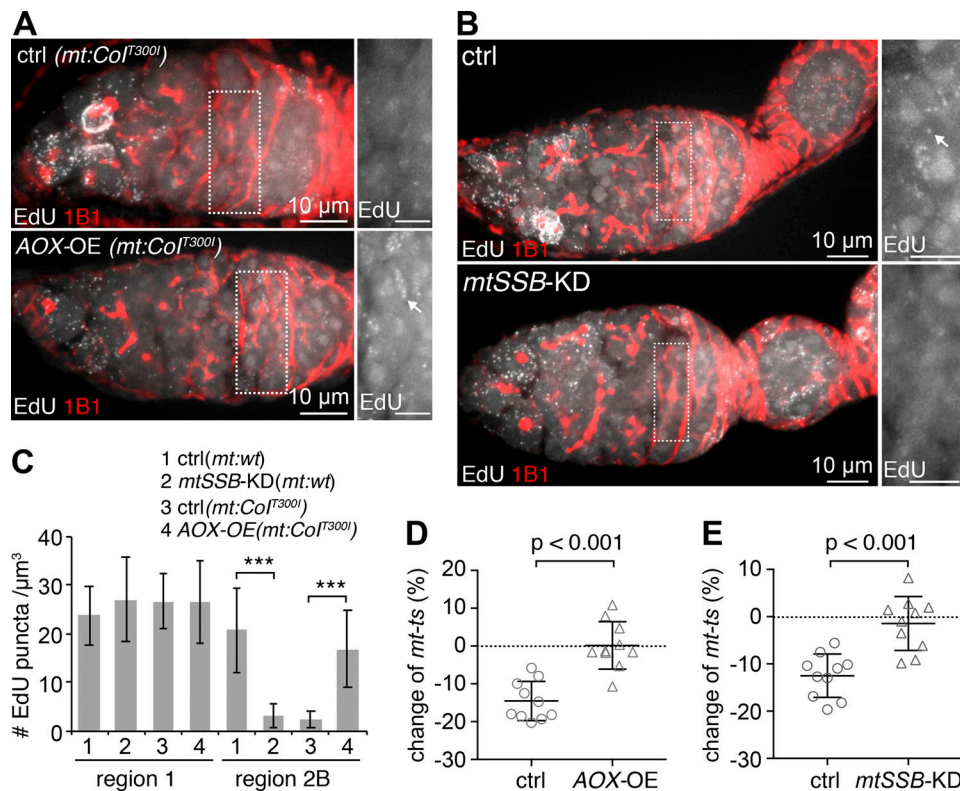


Figure 4. **mtDNA replication is indispensable for selective inheritance.** (A and B) mtDNA replication labeled by EdU staining in germarium. The Hts-1B1 antibody was used to stain the fusome, which indicates the developmental stages of germ cells. Region 2B is outlined in white and enlarged (right panels). Note that the mtDNA replication was specifically disrupted at region 2B in *mt:Col<sup>T3001</sup>* ovary at 29°C but was restored by overexpression of AOX driven by *nanos-gal4* (A). Knocking down *mtSSB* using *nanos-gal4* diminished mtDNA replication at region 2B, but not in egg chambers (B). Arrows point to EdU puncta. Scale bars, 10  $\mu$ m; enlarged images, 5  $\mu$ m. (C) Quantification of mtDNA replication indicated by numbers of EdU puncta in regions 1 and 2B in genetic backgrounds shown in A and B (1, *n* = 11; 2, *n* = 18; 3, *n* = 17; 4, *n* = 20). Data presented are means  $\pm$  SD. \*\*\*, *P* < 0.001. (D and E) Selection against ts mtDNA at 29°C was compromised by ectopic expression of AOX (D) and knockdown of *mtSSB* (E; *n* = 10 for each genotype). Both lines were driven by *nanos-gal4*. Data presented are means  $\pm$  SD. *P* < 0.001.

of which remained at the anterior end (Fig. 5 B). These phenotypes resemble those of a *milton*-null mutant (Cox and Spradling, 2006), indicating the effective disruption of both Milton activity and Balbiani body formation. Of primary importance, the load of ts allele was similar between PGCs and somatic cells in *milton*-knockdown flies (Fig. 5 A), suggesting that the Balbiani body is responsible for the reduction of mutant load in PGCs.

## Discussion

In this study, we illustrate a series of developmentally orchestrated mitochondrial processes in the *Dm* germarium, including mitochondrial fragmentation in dividing cysts, mtDNA expression, and ETC activation in 16-cell cysts at region 2B, that are indispensable for restricting the transmission of deleterious mtDNA mutations (Fig. 6). Using FIB-SEM and computational

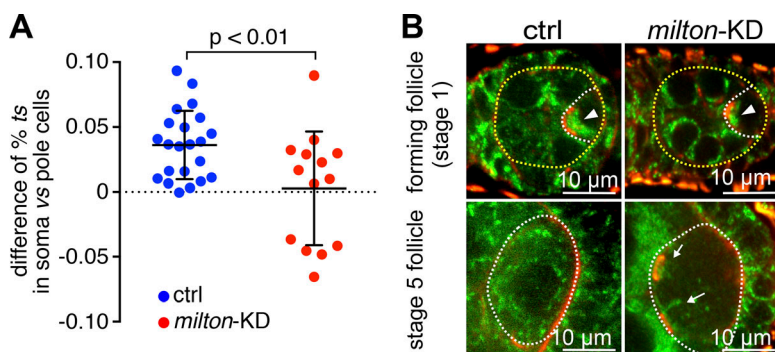
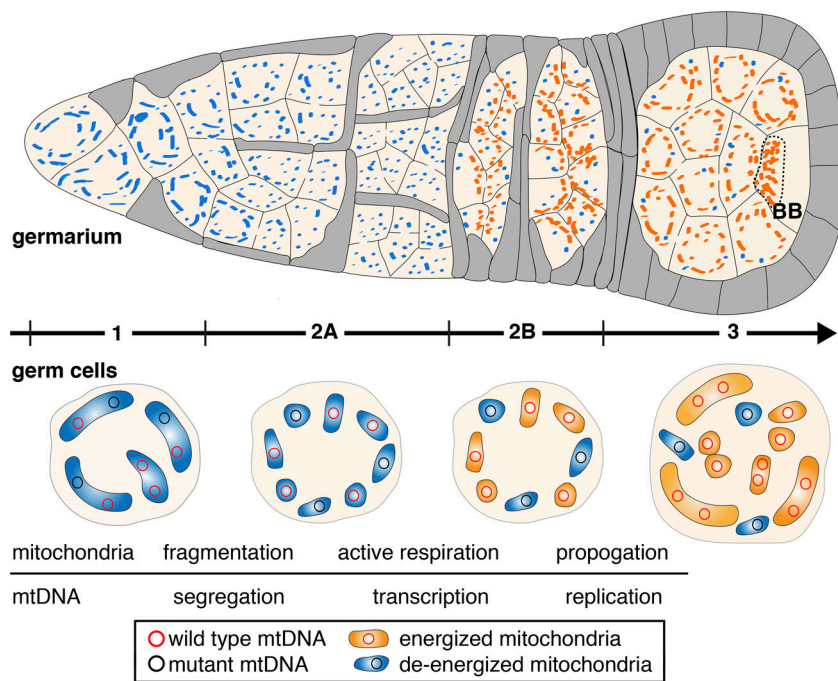


Figure 5. **Balbani body contributes to the reduced mtDNA mutation load in germ cells.** (A) Somatic cells consistently had a higher percentage of ts mtDNA than germ cells (pole cells) in heteroplasmic embryos (*n* = 22). Disrupting the Balbiani body by knocking down *milton* gene (*miltion-KD*) in germ cells abolished the difference between somatic and germ cells (*n* = 14). Data presented are means  $\pm$  SD. *P* < 0.01. (B) Balbiani body formation was disrupted in *milton* knockdown oocytes. Mitochondria labeled by ATPs staining (green), ring canals and actin filaments labeled with phalloidin (red) are shown. In the oocyte (white-dashed outlines) of a forming follicle (yellow-dashed outlines), mitochondria were fewer and remained at the anterior of the oocyte in *milton* knockdown (*miltion-KD*), indicating that the formation of Balbiani body (arrowheads) is impaired. In the oocyte (white-dashed outlines) of wild-type stage 5 egg chamber (ctrl), mitochondria were dispersed evenly in cytoplasm. There were much fewer mitochondria, most of which remained near ring canals (arrows) in *milton* knockdown oocyte. Scale bar, 10  $\mu$ m.





**Figure 6. Developmentally orchestrated mitochondrial processes in *Dm* germarium prime selective inheritance, limiting the transmission of deleterious mtDNA mutations.** Mitochondria are mostly interconnected in the anterior part of the germarium. Mitochondrial fragmentation in dividing cysts, together with the lack of mtDNA replication, promotes mtDNA segregation in dividing cysts and region 2A. The effective mtDNA segregation minimizes the potential complementation among different mitochondrial genotypes. After mtDNA segregation, mtDNA transcription begins, which supports ETC biogenesis and activates mitochondrial respiration in 16-cell cysts at region 2B. The expression of mtDNA hence acts as a stress test for its integrity: mitochondria containing wild-type genome will be active, whereas mitochondria afflicted by deleterious mutations will be depolarized. mtDNA replication begins at region 2B and depends on mitochondrial activity. Healthy mitochondria containing wild-type mtDNA propagate much more vigorously than organelles containing deleterious mutations. These coordinated events act synergistically to restrict the transmission of detrimental mtDNA mutations in the female germline. The Balbiani body (BB) in the oocyte also contributes to selective inheritance by furnishing healthy mitochondria to the germ plasm.

segmentation, we comprehensively documented mitochondrial morphology in the *Dm* germarium. We found that mitochondria displayed a wide range of sizes and shapes in developing germ cells. A subpopulation of elongated, tubular mitochondria in region 1 underwent a drastic morphological change, transitioning to dispersed, rounded organelles in region 2A through Fis1- and Drp1-mediated fission. The mitochondrial fragmentation, together with the lack of mtDNA replication in region 2A, effectively segregates mitochondrial genomes. The chance of potential complementation among different mitochondrial genomes is minimized. In dividing cysts at region 1 and 16-cell cysts at region 2A, where mtDNA segregation took place, mtDNA was not actively transcribed. Progressing into region 2B, mtDNA expression was activated, which triggered the biogenesis of ETCs and the activation of mitochondrial respiration. In heteroplasmic germ cells, mtDNA expression acts as a stress test for the integrity of the mitochondrial genome. Mitochondria harboring wild-type genomes would have functional ETCs and active respiration, whereas mitochondria containing deleterious mutations would have defective ETCs and impaired respiration. At region 2B, mtDNA replication resumes and preferentially takes place in healthy mitochondria (Hill et al., 2014). As a result, the proportion of wild-type genome increases through oogenesis.

In our FIB-SEM analyses, the majority of objects identified by computational segmentation were densely stained, presumably owing to the staining on the inner membrane cristae of mitochondria. We also noticed a minor population of segmented objects that were lightly stained. These objects could be swollen mitochondria, undifferentiated mitochondria that have fewer cristae, or *Wolbachia*. Currently, we were unable to unequivocally call out *Wolbachia*, which have three layers of membranes in host cells (White et al., 2017), owing to the limited resolution of FIB-SEM. Thus, we ran analyses on densely stained objects

only and found the trend of mitochondrial fragmentation to be essentially the same (Fig. 1, C and D vs. Fig. S1, D and E), demonstrating that potential inclusion of *Wolbachia* does not interfere with our analyses. Importantly, *Fis1* knockdown, which should not directly affect *Wolbachia*, effectively shifted the morphology of segmented objects, further supporting our conclusion. However, *Wolbachia* have diverse effects on oogenesis (Werren et al., 2008). It would be appropriate to carry out the same analyses described in this study using *Wolbachia*-free flies to examine the possible effects of *Wolbachia* on mitochondria.

It is known that many nuclear-encoded mitochondrial proteins, including several key factors required for mtDNA replication, are synthesized locally on the mitochondrial surface by cytosolic ribosomes (Zhang et al., 2016). This local translation allows the coupling of synthesis and import of mitochondrial proteins. The import of preproteins across the mitochondrial inner membrane requires mitochondrial membrane potential that depends on active mitochondrial respiration (Geissler et al., 2000). We also found that local translation preferentially takes place on healthy, polarized mitochondria (Zhang et al., 2019). Therefore, unhealthy mitochondria, because of impaired local translation and import, will be starved of nuclear-encoded factors that are essential for mitochondrial biogenesis and mtDNA replication. This may underlie, or at least contribute to, the selective replication of the wild-type genome.

We previously found that mtDNA replication commences in 16-cell cysts at region 2B and is dependent on mitochondrial respiration. Hence, we proposed a model of selective inheritance through replication competition, in which healthy mitochondria containing wild-type genome proliferate much more vigorously and will outcompete those harboring deleterious mutations. This model explains the gradual decline of the load of deleterious mutations over generations (Hill et al., 2014; Ma et al., 2014). In

mouse models, mutations on protein-coding genes that severely affect the mitochondrial respiratory chain activity were eliminated much faster than mild mutations on tRNA genes (Stewart et al., 2008a,b). This observation is consistent with our model of selection based on the functionality of the individual genome, which might represent a conserved mechanism guiding mitochondrial inheritance in metazoans.

We found that healthy mitochondria in the oocytes are pre-selected to join the Balbiani body, which eventually populates the germ plasm in developing embryos. Thus, the Balbiani body enforces a purifying selection to further enhance mitochondrial fitness specifically in germ cells of offspring. This selection likely plays a complementary role and acts synergistically with other mechanisms to further ensure the selective transmission of mtDNA. The exact mechanism of how the healthy mitochondria are predetermined and unevenly distributed in the oocyte is unclear. Given the essential role of Milton in the formation of Balbiani bodies and mtDNA selective inheritance, it is possible that the healthy mitochondria are preferentially transported along the microtubules to the Balbiani body and then localized to the posterior end of oocytes. Balbiani bodies are conserved structures found in developing oocytes across phylogeny (Cox and Spradling, 2003; Pepling et al., 2007; Tworzydło et al., 2016; Zhou et al., 2010). Their roles in mitochondrial inheritance, particularly selective inheritance against damaging mtDNA mutations, remain to be explored in other organisms.

Other models have also been proposed to explain how harmful mtDNA mutations are restricted from transmission through the female germline. Depolarized mitochondria can be cleared through Parkin-PINK1-mediated mitophagy in cultured cells (Narendra et al., 2010). However, neither Parkin (Ma et al., 2014) nor autophagy-related 8-dependent mitophagy is involved in selective inheritance (Lieber et al., 2019; Zhang et al., 2019). A recent study demonstrated that autophagy-related 1 and BCL2 interacting protein 3 (BNIP3) were required for mtDNA selection (Lieber et al., 2019). This new type of selective mitophagy may act in parallel with replication competition to limit the transmission of deleterious mtDNA mutations. However, this potential redundancy cannot explain the complete loss of selection in *mdi* mutants that lack mtDNA replication in ovaries specifically but are largely healthy otherwise (Zhang et al., 2016). It is possible that Mdi may have an unnoted role in BNIP3-mediated mitophagy, which awaits future investigation.

Random segregation of mtDNA, enforced by a mitochondrial bottleneck, in principle could lead to the elimination of unhealthy germ cells or individuals with an excess of damaging mtDNA mutations through Darwinian selection (Stewart and Larsson, 2014). In *Dm*, mtDNA copy number remains constant from PGCs in embryo to GSCs and cystoblasts in pupae (Hurd et al., 2016). In adult germaria region 2A, the absence of mtDNA replication (Hill et al., 2014), greatly reduces mtDNA copy number per germ cell at the 16-cell stage. However, all mitochondria from a 16-cell cyst derived from a single cystoblast end up in the eventual oocyte (Ganguly et al., 2012). Thus, the lack of mtDNA replication in dividing cysts should not be mistakenly considered as a way to generate mitochondrial bottlenecks. We estimate that each GSC contains ~80 nucleoids. This number is

in the range of the calculated value of mitochondria segregation units (Ma et al., 2014). The relatively small number of mtDNA segregation units, together with the large population size, would be sufficient to facilitate the effective segregation of mitochondrial variants in *Dm*. mtDNA mutations that do not severely impair mitochondrial respiration, but only mildly affect other mitochondrial activities, such as reactive oxygen species metabolism or heat production (Wallace, 2005), may not be sensitive to the selective inheritance described in this study. Nonetheless, the random segregation of different mitochondrial haplotypes, and their interactions with both the nuclear genome and environmental factors, would produce progeny with different fitness outcomes. Natural selection on the organismal level would additionally contribute to mtDNA inheritance and evolution (Lajbner et al., 2018; Wallace, 2005).

## Materials and methods

### *Dm* genetics

Flies were maintained on cornmeal medium at 25°C, unless otherwise stated. *w<sup>1118</sup>* was used as the wild-type control. Heteroplasmic *mt:CoI<sup>T300I</sup>* flies were generated previously (Hill et al., 2014) and maintained at 18°C, unless otherwise stated. Generation of the TFAM-GFP reporter lines was described previously (Zhang et al., 2016). The UASp-AOX transgenic fly was generated by subcloning the *Ciona intestinalis* AOX coding sequence into the pUASp vector (Rørth, 1998), followed by standard germline transformation procedures (Chen et al., 2015). UASp-mitoGFP transgenic fly was generated by cloning a fusion gene consisting of the N-terminal 40 amino acid residues of *Dm* citrate synthase (CG3861) and EGFP cDNA into the pUASp vector, followed by standard germline transformation procedures. *Fis1* RNAi (BL#63027), *cox5A* RNAi (BL#58282), *mtSSB* RNAi lines (BL#50600), *milton* RNAi (BL#43173), X-linked *mChFP-Rho1* (BL#52280), *bam-gal4* (BL#80579), and *nanos-gal4* (BL#4937) were from the Bloomington Drosophila Stock Center. *Drp1* RNAi (v44156) and *tamas* RNAi (v3135) were from Vienna Drosophila Resource Center. *Vasa-GFP* (#109171) came from Kyoto Drosophila Genomics and Genetics Resources.

### *Dm* fecundity and hatching rate

To assay *Dm* fecundity, female flies of various genotypes were collected as virgins and crossed with young *w<sup>1118</sup>* male flies. Each vial contained three female and five male flies. The flies were transferred to a fresh vial every other day for 3 wk. The mean number of eggs produced by each female per day was calculated. Each genotype was replicated 15 times. For assaying the hatching rate, virgin flies of various genotypes were crossed with young *w<sup>1118</sup>* male flies in batches. Approximately 150 embryos were collected overnight and placed in groups of 20 on molasses plates with a small amount of yeast paste in the center. Plates were incubated at 25°C for 2 d. The number of larvae was counted and normalized to the total number of embryos to determine the hatching rate.

### Immunostaining of *Dm* germ cells

For staining of adult ovaries, 1–2-d-old females were fed with yeast overnight before analysis. Ovaries were dissected in

Schneider's medium supplemented with 10% FBS (Gibco) at room temperature. Ovaries were fixed for 20 min in 3.7% PFA (Electron Microscopy Sciences) in PBS, then permeabilized in PBS containing 0.5% Triton X-100. After blocking in PBSBT buffer (1× PBS, 0.1% Triton X-100, and 0.2% BSA), the ovaries were incubated with primary antibodies overnight at 4°C. After washing with PBSBT buffer three times, the ovaries were incubated with secondary antibodies at room temperature for 1 h and washed again with PBSBT buffer three times. Each ovariole was separated with fine-nose forceps under the stereomicroscope and mounted with Prolong Glass antifade mounting medium (Invitrogen) on the slides. Confocal images were collected on a PerkinElmer Ultraview system (Zeiss Plan-apochromat 63×/1.4 oil lens, Volocity acquisition software, Hamamatsu Digital Camera C10600 ORCA-R2, Immersol immersion oil).

Antibodies used were as follows: mouse ATP synthase subunit  $\alpha$  (Abcam, 15H4C4, 1:1,000), rat  $\alpha$ -Vasa (Developmental Studies Hybridoma Bank, 1:200), rabbit  $\alpha$ -GFP (Novus Biologicals, NB600-308, 1:1,000); Hts-1B1 (Developmental Studies Hybridoma Bank, 1:200); Alexa Fluor 647-Phalloidin (Invitrogen, 1:50); Alexa Fluor 568 goat  $\alpha$ -rat IgG (Invitrogen, 1:200), Alexa Fluor 568 goat  $\alpha$ -mouse IgG (Invitrogen, 1:200), Alexa Fluor 568 goat  $\alpha$ -rabbit IgG (Invitrogen, 1:200), and Atto 647N goat  $\alpha$ -rabbit IgG (Sigma-Aldrich, 1:200).

### STED microscopy and imaging quantification

A Leica SP8 3× STED microscope (Leica 100×/1.4 STED White objective, LAS X software, Immersol immersion oil) was used for imaging germaria stained for ATPs (Alexa Fluor 568  $\alpha$ -mouse IgG) and TFAM-GFP (Atto 647N goat  $\alpha$ -rabbit IgG). Huygens deconvolution algorithm was used for the deconvolution of raw STED images. 3D stack images (10  $\mu\text{m}$  of z-stack and 0.16  $\mu\text{m}$ /z-step) were analyzed with ImageJ (National Institutes of Health). Cells from different germarium regions were selected manually by “freehand selection” function and isolated by “duplicate” function. Fluorescence outside the selected cell regions was removed by “clear outside” function. Background fluorescence value from each cell image was determined from a  $1.5 \times 1.5\text{-}\mu\text{m}^2$  region in the nucleus and subtracted from the original cell image by using “math-subtract” function. Individual mitochondrion and nucleoid from ATPs and TFAM-GFP channels, respectively, were called out using “color threshold” function with a “MaxEntropy” thresholding setting. Fluorescence outside the outlined ATPs and TFAM-GFP regions was removed by “clear outside” function. Next, we used a “restore selection” function to copy the outlined TFAM-GFP particle regions into the corresponding ATPs image. Then, the nucleoid number per mitochondrion was calculated manually as the number of outlined TFAM-GFP particles in an outlined ATPs particle. TFAM-GFP marking nucleoids does not always display a round dot shape. Instead, some puncta showed a connection in between to form peanut-shape staining, which may reflect different compaction states of mtDNA. To address this, 8-bit binary images for TFAM-GFP staining were generated using the “make binary” function and further refined using a “watershed” function integrated in ImageJ to separate touching TFAM-GFP objects. After background removal and “clear outside” processing,

nonmitochondria areas had zero fluorescence intensity; thus a single mitochondrion was defined as ATPs staining with continuous pixels of fluorescence intensity. We noticed that the ATPs staining was not always uniform, with less intensity in the regions where nucleoids were located, which could be due to a lack of cristae structures surrounding nucleoids (Stephan et al., 2019). Thus, a single mitochondrion was called if two adjacent but distinct ATs puncta were connected with a single nucleoid. We found that there were  $\sim 10\%$  TFAM-GFP puncta in the cell localized in clustered mitochondria, which could not be individualized by ImageJ. This population of TFAM-GFP puncta was excluded from quantification.

### 3D volume FIB-SEM

FIB-SEM was performed as previously described, with modifications (Bleck et al., 2018). Ovaries were dissected in Schneider's medium supplemented with 10% FBS (Gibco) and immediately fixed in fixation solution (2.5% glutaraldehyde, 2% formaldehyde, and 2 mM calcium chloride in 0.1 M sodium cacodylate buffer) at room temperature for 5 min, followed by an additional fixation on ice for 3 h. After washing in cold cacodylate buffer containing 2 mM calcium chloride, the ovaries were postfixed with reduced 2%  $\text{Os}_2\text{O}_4$  (reduced by 1.5% potassium ferrocyanide right before use) for 1 h on ice. After washing with water, the tissues were placed in the thiocarbonylhydrazide solution for 20 min at room temperature. Then, the ovaries were fixed in 2%  $\text{Os}_2\text{O}_4$  for 30 min at room temperature, stained en bloc with 1% uranyl acetate overnight at 4°C, and further stained with Walton's lead aspartate solution for 30 min at 60°C. After dehydration with ethanol series, the samples were embedded in Durcupan ACM resin (Electron Microscopy Sciences).

Embedded samples were faced with a trim tool 90 diamond knife (DIATOME) on a Leica UCF-7 ultramicrotome and sputter-coated with palladium/gold at a thickness of 50 nm in an EMS 575X sputter coater (Electron Microscopy Sciences). The samples were imaged using a Crossbeam 540 FIB-SEM microscope (Carl Zeiss Microscopy). Platinum and carbon pads were deposited over the region of interest (ROI), and the run was set up and controlled by Atlas 5 software (Fibics). SEM images were acquired using an accelerating 1.5-keV beam with a 1.5-nA beam current, and the in-lens detector captured backscattered electrons. The milling was performed with a FIB operating at 30 keV with a beam current of 700 pA. The slice thickness and imaging pixel size were set to  $10 \times 10 \times 10\text{-nm}$  voxels. The total volume acquired per tissue sample was, for wild-type,  $29.59 \times 26.19 \times 30.30\text{ }\mu\text{m}$  (XYZ); and for *Fis1* knockdown,  $29.06 \times 31.67 \times 19.29\text{ }\mu\text{m}$  (XYZ). The milling was performed from the anterior tip of the germaria toward the posterior.

### Segmentation of mitochondria and cell clusters

Image segmentation was completed on a desktop PC (Thinkmate) running Windows 10 with Intel Xeon Gold 6254 3.10 GHz processors, 2.0 TB RAM, and an NVIDIA Titan V 12 GB VRAM video card. We used Dragonfly software (v4.1; Object Research Systems) to segment the mitochondria and cells and collect mitochondrial morphometric information. Segmentation of mitochondria was completed using the U-Net convolutional



neural network within the deep-learning tool in Dragonfly (Ronneberger et al., 2015). We used six raw FIB-SEM images from evenly distributed regions (approximately one image every 400 steps) of the wild-type sample to build our mitochondrial training set for the U-Net model. Mitochondria were initially segmented by labeling the outer mitochondrial membrane (OMM) via thresholding followed by manual clean-up. Next, the mitochondrial matrix was segmented using the fill inner area tool of the OMM ROI, followed by the erode tool and manual cleaning to eliminate the OMM ROI. We used this training dataset to build the U-net model where training data were augmented (horizontal and vertical flip, 180° max rotation, 10° max shear, 75–150% scale, 0–2 brightness, and 0–0.10 Gaussian noise), and 20% of the training data were used for validation. We used categorical cross-entropy for our loss function and Adadelta for our optimization algorithm. The model was then applied to the full volume to segment out the mitochondrial matrix, which was then manually cleaned.

To segment individual mitochondria, we used a watershed mapping approach. Watershed map seed points were isolated from the previously described mitochondrial matrix ROIs using a connected components analysis. The boundaries of this watershed map were set by the OMM, which was included by dilating the mitochondrial matrix ROI, followed by manual cleaning. To filter out the potential contamination by *Wolbachia* (Ferre et al., 2005), we used a screen for mean voxel intensity and manually filtered the results.

In FIB-SEM images, the size of nuclei and locations of cells were used to distinguish germ cells from somatic cells. For germ cells, their relative locations in a germarium, and the number of interconnected germ cells, judged by presence of ring canals and connecting fusome within a cyst, were used to determine their developmental stage. Cell clusters were segmented from the 3D volume using z-interpolation over 50 image intervals. Cell cluster-specific mitochondrial surface area and volume were extracted from these datasets.

### Membrane potential staining

Adult ovaries were dissected in Schneider's medium supplemented with 10% FBS and incubated with medium containing TMRM (Invitrogen, 1:1,000) and MitoTracker green (Invitrogen, 100 nM) for 20 min. The ovaries were rinsed with PBS three times and imaged live on a PerkinElmer Ultraview system (Zeiss Plan-apochromat 63×/1.4 oil lens, Volocity acquisition software, Hamamatsu Digital Camera C10600 ORCA-R2, Immersol immersion oil) within 1 h. The position and morphological characters were used to define developmental stages of germ cells. The 16-cell cyst at region 2B is flattened and extends the entire width of the germarium. Mitochondria are closely associated with fusome in this region; thus the mitochondrial staining within the cyst at this stage displays a long, branched appearance along the fusome structures. Region 2A cysts are considered as locating immediately anterior of the first region 2B cyst.

To generate ratiometric images of TMRM/MitoTracker green, z-stack images (4 steps with 0.5 μm/z-step) were analyzed with ImageJ. Each channel was separated. Regions of mitochondria were selected on the MitoTracker green channel

with the “color threshold” function at default settings. “Restore selection” function was applied to outline mitochondrial area on the corresponding TMRM channel. Fluorescence outside mitochondria (background) was removed from both channels with “clear outside” function. The ratiometric images were generated with “Image Calculator” function by normalizing the intensity of TMRM with that of MitoTracker green.

### Mitochondrial activity staining in *Dm* adult ovaries

Histochemical staining for the activity of mitochondrial succinate dehydrogenase (complex II) and cytochrome c oxidase (complex IV) in ovaries was performed as previously described, with modifications (Wang et al., 2019). Ovaries were dissected in PBS and incubated in cytochrome c oxidase assay medium (100 μM cytochrome c, 4 mM diaminobenzidine tetrahydrochloride, and 20 μg/ml catalase in 0.2 M phosphate buffer, pH 7.0) at room temperature for 30 min. The ovaries were then washed in PBS three times and incubated in succinate dehydrogenase assay medium (130 mM sodium succinate, 200 μM phenazine methosulphate, 1 mM sodium azide, and 1.5 mM nitroblue tetrazolium in 0.2 M phosphate buffer, pH 7.0) at room temperature for 10 min. After washing in PBS three times, ovaries were dehydrated in a graded ethanol series (70%, 95%, 2 × 100%), cleared in Histoclear (National Diagnostics) for 15 min, and mounted in dibutyl phthalate in xylene (VWR) overnight. Bright-field images were collected on a Zeiss Axio Observer Z1 microscope (Objective C-Apochromat 40×/1.1 W Corr, Leica LAS EZ software, Leica EC4 Digital Camera, water as immersion medium).

### EdU labeling in *Dm* adult ovaries

EdU incorporation assay in *Dm* ovaries was performed as described (Hill et al., 2014). Briefly, adult ovaries were dissected in Schneider's medium supplemented with 10% FBS (Gibco) and pretreated with 7 μM aphidicolin (Sigma-Aldrich) diluted in the same medium for 3 h at room temperature. The ovaries were incubated with 10 μM EdU and 7 μM aphidicolin in Schneider's medium with 10% FBS for 2 h. After washing with Schneider's medium 3 times, ovaries were fixed in 4% PFA in PBS for 20 min at room temperature. Tissues were then washed twice in washing buffer (PBS and 3% BSA) for 5 min and permeabilized with 0.5% Triton X-100 in PBS for 20 min. The Click-iT EdU labeling kit (Invitrogen) was used to label EdU according to the manufacturer's instructions. The tissues were washed twice with PBS washing buffer and blocked in PBSBT for 30 min. The ovaries were costained with fusome antibody to define developmental stages of germ cells. Incubation with primary antibody was performed overnight at 4°C, followed by the immunostaining procedures described above.

### Single-molecule FISH (smFISH) and quantification

The mitochondrial and nuclear-encoded transcripts in the germarium were detected using an smFISH protocol published previously (Trcek et al., 2017). Briefly, dissected ovaries were fixed in 4% PFA in PBS for 20 min. After washing with PBST (PBS and 0.2% Triton X-100) five times for 5 min each, ovaries were treated with 3 μg/ml proteinase K in PBS on ice for 1 h. Ovaries were incubated with 20 mg/ml glycine to stop

proteinase K digestion and were postfixed in 4% PFA in PBST for 20 min. After washing with PBST five times for 2 min each, ovaries were incubated in prehybridization solution (2× SSC and 10% formamide) at room temperature for 10 min. Prehybridization solution was removed, and 60 μl of hybridization solution (6 μl deionized formamide, 1 μl heparin, 1 μl salmon sperm DNA, 80 ng probe mix, 6 μg dextran sulfate, 120 μg BSA, and 5 μl of 20× SSC) was added. Ovaries were protected from light and incubated at 37°C overnight. Ovaries were then washed with prewarmed prehybridization solution twice for 15 min each time in a 37°C incubator, followed by washing with PBS twice for 5 min each time at room temperature. Series images with FISH and nuclear (DAPI) channels were collected by an Instant Sim (iSIM) Super-Resolution Microscope (Olympus UPlanApo 100×/1.50 oil lens, Metamorph acquisition software, ORCA-Flash4.0 V2 Digital CMOS camera C11440, IMMOIL-F30CC immersion oil). Microvolution software was applied to deconvolve iSIM images using measured point spread function. The sequence of fluorescently labeled short DNA probes targeting to *ND4*, *CoI*, *ND-SGDH*, *cox5A*, *Fis1*, *Drp1*, and *mtSSB* mRNA are listed in Table S2.

Germline cells and germarium regions were identified based on position, morphological characters, and nucleus size (DAPI staining). Nuclei of region 2B germ cells are round and surrounded by prefollicle cells that have smaller oval or round nuclei. Region 2A cysts are located immediately anterior of the first region 2B cyst. To quantify relative mRNA levels of *ND4*, *ND-SGDH*, *CoI*, or *cox5A* in the region 2A and 2B cysts (Fig. 3 B), cysts from germarium region 2A and 2B were manually outlined, duplicated to display as two different images with the “Duplicate” function, and isolated by the “clear outside” function, respectively. The “3D objects counter” plugin at the smallest threshold setting was used to select the whole cyst region and quantify cyst volume from each series image. The “3D objects counter” plugin with automatic threshold setting was used to select and quantify fluorescence intensity of each FISH punctum in 3D. Background fluorescence value was subtracted from total FISH fluorescence intensity in each germarium region. The resulting net FISH fluorescence intensity was divided by the corresponding cyst volume.

RNAi for *Fis1*, *Drp1*, *cox5A*, and *mtSSB* was performed specifically in the germ cells. The abundance of these transcripts in the follicle cells should not be affected. Therefore, we used the smFISH fluorescence intensity in follicle cells as an internal control to determine the knockdown efficiency of each RNAi line. In ImageJ, the areas of region 2A cysts (for *Fis1* and *Drp1* RNAi) or region 2B cysts (for *cox5A* and *mtSSB* RNAi), and their corresponding region 2B follicle cells, were manually outlined. The fluorescence intensity from each selected region was calculated with the method described above. The resulting smFISH fluorescence intensity from region 2A or 2B cysts were normalized by that of the corresponding region 2B follicle cells.

#### PGC isolation from *Dm*

The PGCs from *Dm* embryos and pupae were isolated as previously described (Shigenobu et al., 2006), with modifications. A Vasa-GFP transgene that specifically labels germ cells

throughout the life cycle was used to isolate the germ cells using FACS. Female PGCs were separated from male PGCs with an X-chromosome-linked monomeric cherry fluorescence (mChFP)-tagged Rho1 protein under control of Rho1 regulatory sequence (Abreu-Blanco et al., 2014). The female Vasa-GFP transgenic flies, which carry wild-type or heteroplasmic *mt:CoI<sup>T300I</sup>* mtDNA, were crossed with male X-linked mChFP-Rho1 flies in cages and allowed to lay eggs on a grape agar plate (Genesee Scientific). The germ cells of the female progeny carry both GFP and mChFP fluorescence. After precollection for 3 h, the embryos were collected and allowed to develop till stage 15 at 25°C (staging according to Williamson and Lehmann [1996]). The embryos were then dechorionated for 30 s in 50% bleach. After washing with water, the embryos were transferred to a microcentrifuge tube filled with 500 μl of Schneider’s insect medium (Gibco). The blue pestle matching with the microcentrifuge tube (USA Scientific) was used to gently homogenize the embryos. The homogenate was filtered through a 125-μm mesh and centrifuged at 860 g for 1 min at 4°C. After one wash in ice-cold calcium-free Schneider’s medium (Sigma-Aldrich), the pellet was resuspended in calcium-free Schneider’s medium containing 0.25% trypsin (Invitrogen) and incubated at 37°C for 10 min. The cell suspension was filtered through a 35-μm mesh, and the same amount of Schneider’s medium supplemented with 20% FBS was added to stop the trypsinization. The dissociated cells were pelleted by centrifugation at 860 g for 1 min. The cells were resuspended in Schneider’s medium and filtered through a 35-μm mesh immediately before cell sorting. Flow cytometry analyses were performed on a BD FACSCalibur flow cytometer and analyzed with FACSDiva. The female PGCs were sorted by gating for GFP- and mChFP-positive events. Female somatic cells were sorted by gating for GFP-negative and mChFP-positive events. The quality and purity of the sorted PGCs were confirmed by fluorescence microscope. For isolation of PGCs from pupae, the staged embryos were transferred to the standard cornmeal medium until the desired development stage. All the other procedures were the same except for the exclusion of the dechorionation step.

#### *Dm* ovaries stem cell culture

The fGS/OSS is a stable cell line consisting of a mixture of *Dm* adult fGSs and ovarian somatic sheath cells (OSSs). OSS is the derivative line, in which the fGS component has been lost. Both cell lines were obtained from Drosophila Genomics Resource Center and cultured as described previously (Niki et al., 2006).

#### Measurement of mtDNA copy number

To quantify mtDNA copy number, total DNA was isolated from the FACS-sorted PGCs or the somatic cells using QIAamp DNA Micro Kit (Qiagen). The mtDNA copy number was measured using droplet digital PCR (ddPCR, Bio-Rad), a method for absolute quantification of nucleic acids. Primers were targeted to the mtDNA-encoded cytochrome c oxidase subunit I (*CoI*) and the nuclear-encoded Histone 4 (*His4*) genes. Primers and probes used in ddPCR are as follows: *CoI*: forward, 5'-ATTGGAGTTAAT TTAACATTTTTTCTCA-3'; reverse, 5'-AGTTGATACAATATTT CATGTTGTGTAAG-3'; probe, 5'-AATACCTCGACGTTATTCAGA

TTACCCA-3'; His4: forward, 5'-TCCAAGGTATCACGAAGCC-3'; reverse, 5'-AACCTTCAGAACGCCAC-3'; and probe, 5'-AGCGCA TATCTGGACTCATATACGAG-3'.

The CoI and His4 probes were synthesized by labeling the 5' nucleotide with FAM and HEX reporter fluorophores, respectively. Approximately 1 µg of total DNA was digested with EcoRI at 37°C for 1 h. Then the ddPCR reaction mixture was assembled to contain 1× ddPCR Supermix for probes (Bio-Rad), 900 nM of each forward and reverse primer, 250 nM of probe, and ≤1 ng of total DNA. The reaction was conducted in the QX200 Droplet Generator, followed by the thermal cycler, and analyzed by the QX200 Droplet reader per the manufacturer's instructions.

#### mtDNA selection and quantification of heteroplasmy

mtDNA selection in the female germline was performed according to a previous study (Zhang et al., 2019). Briefly, heteroplasmic flies with wild-type and knockdown nuclear backgrounds were transferred from 18°C to 29°C right after eclosion. An individual heteroplasmic female fly was mated with five male *w<sup>1118</sup>* flies at 29°C, and ≥10 female flies were analyzed. Eggs produced during the first 6 d were discarded. The eggs laid on day 7 were pooled, and the heteroplasmic levels were compared between mother and eggs. Quantification of heteroplasmic mtDNA was performed as described previously (Hill et al., 2014).

#### Statistical analysis

Data were analyzed using Student's *t* test, Mann-Whitney *U* test, or one-way analysis of variance. The difference was considered statistically significant when *P* < 0.05.

#### Online supplemental material

Fig. S1 shows the change of mitochondrial volume and morphology in early germarium by FIB-SEM. Fig. S2 shows the expression pattern of germline-specific drivers and the knockdown efficiency of several RNAi lines. Fig. S3 shows the quantification of mtDNA copy number in GSCs. Fig. S4 shows that knockdown of *Drp1* impairs nucleoid segregation and mtDNA selective inheritance; knockdown of *tamas* in ovary diminished mtDNA selection. Fig. S5 shows *Dm* fecundity and hatching rate of several RNAi lines. Video 1 and Video 2 show 3D FIB-SEM image stacks of wild-type (Video 1) and *Fis1* knockdown (Video 2) *Dm* germarium with automated mitochondrial segmentation. Table S1 shows the frequency distribution of mitochondrial volume in control and *Fis1* knockdown germarium. Table S2 shows the sequence of FISH short DNA probes.

#### Acknowledgments

We thank F. Chanut for comments and edits on the manuscript; B. Glancy for advice and comments on the FIB-SEM work; M. Aronova and J. Cohen for EM technical assistance; National Heart, Lung, and Blood Institute FACS core and National Cancer Institute Center for Cancer Research Genomics core for technical support; Bloomington *Drosophila* Stock Center, Vienna *Drosophila* Resource Center, Kyoto *Drosophila* Genomics and Genetics Resources for fly stocks; *Drosophila* Genomics Resource

Center for *Dm* stem cell cultures; and Developmental Studies Hybridoma Bank for antibodies. We are also grateful to the managing editor and anonymous reviewers for their comments and suggestions on the manuscript.

This work was supported by the National Heart, Lung, and Blood Institute Intramural Research Program.

The authors declare no competing financial interests.

Author contribution: H. Xu and Z. Chen conceived and designed the project and prepared the manuscript. Z. Chen performed the fly genetics, mtDNA inheritance, PGC isolation and quantification, mitochondrial activity, and EdU labeling assays. Z.H. Wang performed the smFISH, iSIM imaging, mitochondrial membrane potential, image quantification, and data analyses. Z.H. Wang and C. Combs carried out the STED imaging. Z. Chen and G. Zhang prepared samples for FIB-SEM. C.K.E. Bleck and E. Lindberg performed 3D Volume FIB-SEM. D.J. Chung and G. Madison did mitochondrial segmentation and data analyses on FIB-SEM. R.S. Balaban provided FIB-SEM analysis support. H. Xu supervised the project.

Submitted: 22 May 2019

Revised: 15 November 2019

Accepted: 10 April 2020

#### References

- Abreu-Blanco, M.T., J.M. Verboon, and S.M. Parkhurst. 2014. Coordination of Rho family GTPase activities to orchestrate cytoskeleton responses during cell wound repair. *Curr. Biol.* 24:144–155. <https://doi.org/10.1016/j.cub.2013.11.048>
- Alam, T.I., T. Kanki, T. Muta, K. Ukaji, Y. Abe, H. Nakayama, K. Takio, N. Hamasaki, and D. Kang. 2003. Human mitochondrial DNA is packaged with TFAM. *Nucleic Acids Res.* 31:1640–1645. <https://doi.org/10.1093/nar/gkg251>
- Bleck, C.K.E., Y. Kim, T.B. Willingham, and B. Glancy. 2018. Subcellular connectomic analyses of energy networks in striated muscle. *Nat. Commun.* 9:5111. <https://doi.org/10.1038/s41467-018-07676-y>
- Chan, D.C.. 2006. Mitochondria: dynamic organelles in disease, aging, and development. *Cell.* 125:1241–1252. <https://doi.org/10.1016/j.cell.2006.06.010>
- Chen, D., and D.M. McKearin. 2003. A discrete transcriptional silencer in the *bam* gene determines asymmetric division of the *Drosophila* germline stem cell. *Development.* 130:1159–1170. <https://doi.org/10.1242/dev.00325>
- Chen, Z., Y. Qi, S. French, G. Zhang, R. Covian Garcia, R. Balaban, and H. Xu. 2015. Genetic mosaic analysis of a deleterious mitochondrial DNA mutation in *Drosophila* reveals novel aspects of mitochondrial regulation and function. *Mol. Biol. Cell.* 26:674–684. <https://doi.org/10.1091/mbc.E14-11-1513>
- Cox, R.T., and A.C. Spradling. 2003. A Balbiani body and the fusome mediate mitochondrial inheritance during *Drosophila* oogenesis. *Development.* 130:1579–1590. <https://doi.org/10.1242/dev.00365>
- Cox, R.T., and A.C. Spradling. 2006. Milton controls the early acquisition of mitochondria by *Drosophila* oocytes. *Development.* 133:3371–3377. <https://doi.org/10.1242/dev.02514>
- Cree, L.M., D.C. Samuels, S.C. de Sousa Lopes, H.K. Rajasimha, P. Wonnapijit, J.R. Mann, H.H. Dahl, and P.F. Chinnery. 2008. A reduction of mitochondrial DNA molecules during embryogenesis explains the rapid segregation of genotypes. *Nat. Genet.* 40:249–254. <https://doi.org/10.1038/ng.2007.63>
- Fan, W., K.G. Waymire, N. Narula, P. Li, C. Rocher, P.E. Coskun, M.A. Vannan, J. Narula, G.R. Macgregor, and D.C. Wallace. 2008. A mouse model of mitochondrial disease reveals germline selection against severe mtDNA mutations. *Science.* 319:958–962. <https://doi.org/10.1126/science.1147786>
- Felsenstein, J.. 1974. The evolutionary advantage of recombination. *Genetics.* 78:737–756.



- Ferree, P.M., H.M. Frydman, J.M. Li, J. Cao, E. Wieschaus, and W. Sullivan. 2005. Wolbachia utilizes host microtubules and Dynein for anterior localization in the *Drosophila* oocyte. *PLoS Pathog.* 1: e14. <https://doi.org/10.1371/journal.ppat.0010014>
- Frank, S., B. Gaume, E.S. Bergmann-Leitner, W.W. Leitner, E.G. Robert, F. Catez, C.L. Smith, and R.J. Youle. 2001. The role of dynamin-related protein 1, a mediator of mitochondrial fission, in apoptosis. *Dev. Cell.* 1:515–525. [https://doi.org/10.1016/S1534-5807\(01\)00055-7](https://doi.org/10.1016/S1534-5807(01)00055-7)
- Ganguly, S., L.S. Williams, I.M. Palacios, and R.E. Goldstein. 2012. Cytoplasmic streaming in *Drosophila* oocytes varies with kinesin activity and correlates with the microtubule cytoskeleton architecture. *Proc. Natl. Acad. Sci. USA.* 109:15109–15114. <https://doi.org/10.1073/pnas.1203575109>
- Geissler, A., T. Krimmer, U. Bömer, B. Guiard, J. Rassow, and N. Pfanner. 2000. Membrane potential-driven protein import into mitochondria. The sorting sequence of cytochrome b(2) modulates the deltapendency of translocation of the matrix-targeting sequence. *Mol. Biol. Cell.* 11:3977–3991. <https://doi.org/10.1091/mbc.11.11.3977>
- Gilkinson, R.W., E.A. Schon, E. Hernandez, and M.M. Davidson. 2008. Mitochondrial nucleoids maintain genetic autonomy but allow for functional complementation. *J. Cell Biol.* 181:1117–1128. <https://doi.org/10.1083/jcb.200712101>
- Harris, L.K., and J.A. Theriot. 2018. Surface Area to Volume Ratio: A Natural Variable for Bacterial Morphogenesis. *Trends Microbiol.* 26:815–832. <https://doi.org/10.1016/j.tim.2018.04.008>
- Hauswirth, W.W., and P.J. Laipis. 1982. Mitochondrial DNA polymorphism in a maternal lineage of Holstein cows. *Proc. Natl. Acad. Sci. USA.* 79:4686–4690. <https://doi.org/10.1073/pnas.79.15.4686>
- Hill, J.H., Z. Chen, and H. Xu. 2014. Selective propagation of functional mitochondrial DNA during oogenesis restricts the transmission of a deleterious mitochondrial variant. *Nat. Genet.* 46:389–392. <https://doi.org/10.1038/ng.2920>
- Hurd, T.R., B. Herrmann, J. Sauerwald, J. Sanny, M. Grosch, and R. Lehmann. 2016. Long Oskar Controls Mitochondrial Inheritance in *Drosophila melanogaster*. *Dev. Cell.* 39:560–571. <https://doi.org/10.1016/j.devcel.2016.11.004>
- Ishihara, N., Y. Fujita, T. Oka, and K. Mihara. 2006. Regulation of mitochondrial morphology through proteolytic cleavage of OPA1. *EMBO J.* 25:2966–2977. <https://doi.org/10.1038/sj.emboj.7601184>
- Jenuth, J.P., A.C. Peterson, K. Fu, and E.A. Shoubridge. 1996. Random genetic drift in the female germline explains the rapid segregation of mammalian mitochondrial DNA. *Nat. Genet.* 14:146–151. <https://doi.org/10.1038/ng1096-146>
- Korhonen, J.A., X.H. Pham, M. Pellegrini, and M. Falkenberg. 2004. Reconstitution of a minimal mtDNA replisome in vitro. *EMBO J.* 23:2423–2429. <https://doi.org/10.1038/sj.emboj.7600257>
- Kukat, C., C.A. Wurm, H. Spähr, M. Falkenberg, N.G. Larsson, and S. Jakobs. 2011. Super-resolution microscopy reveals that mammalian mitochondrial nucleoids have a uniform size and frequently contain a single copy of mtDNA. *Proc. Natl. Acad. Sci. USA.* 108:13534–13539. <https://doi.org/10.1073/pnas.1109263108>
- Labrousse, A.M., M.D. Zappaterra, D.A. Rube, and A.M. van der Bliek. 1999. C. elegans dynamin-related protein DRP-1 controls severing of the mitochondrial outer membrane. *Mol. Cell.* 4:815–826. [https://doi.org/10.1016/S1097-2765\(00\)80391-3](https://doi.org/10.1016/S1097-2765(00)80391-3)
- Lajbner, Z., R. Pnini, M.F. Camus, J. Miller, and D.K. Dowling. 2018. Experimental evidence that thermal selection shapes mitochondrial genome evolution. *Sci. Rep.* 8:9500.
- Legros, F., F. Malka, P. Frachon, A. Lombès, and M. Rojo. 2004. Organization and dynamics of human mitochondrial DNA. *J. Cell Sci.* 117:2653–2662. <https://doi.org/10.1242/jcs.01134>
- Lieber, T., S.P. Jeedigunta, J.M. Palozzi, R. Lehmann, and T.R. Hurd. 2019. Mitochondrial fragmentation drives selective removal of deleterious mtDNA in the germline. *Nature.* 570:380–384. <https://doi.org/10.1038/s41586-019-1213-4>
- Ma, H., H. Xu, and P.H. O'Farrell. 2014. Transmission of mitochondrial mutations and action of purifying selection in *Drosophila melanogaster*. *Nat. Genet.* 46:393–397. <https://doi.org/10.1038/ng.2919>
- Narendra, D.P., S.M. Jin, A. Tanaka, D.F. Suen, C.A. Gautier, J. Shen, M.R. Cookson, and R.J. Youle. 2010. PINK1 is selectively stabilized on impaired mitochondria to activate Parkin. *PLoS Biol.* 8: e1000298. <https://doi.org/10.1371/journal.pbio.1000298>
- Niki, Y., T. Yamaguchi, and A.P. Mahowald. 2006. Establishment of stable cell lines of *Drosophila* germ-line stem cells. *Proc. Natl. Acad. Sci. USA.* 103:16325–16330. <https://doi.org/10.1073/pnas.0607435103>
- Olivo, P.D., M.J. Van de Walle, P.J. Laipis, and W.W. Hauswirth. 1983. Nucleotide sequence evidence for rapid genotypic shifts in the bovine mitochondrial DNA D-loop. *Nature.* 306:400–402. <https://doi.org/10.1038/306400a0>
- Pepling, M.E., J.E. Wilhelm, A.L. O'Hara, G.W. Gephardt, and A.C. Spradling. 2007. Mouse oocytes within germ cell cysts and primordial follicles contain a Balbiani body. *Proc. Natl. Acad. Sci. USA.* 104:187–192. <https://doi.org/10.1073/pnas.0609923104>
- Rebolledo-Jaramillo, B., M.S. Su, N. Stoler, J.A. McElhoe, B. Dickins, D. Blankenberg, T.S. Korneliusen, F. Chiaromonte, R. Nielsen, M.M. Holland, et al. 2014. Maternal age effect and severe germ-line bottleneck in the inheritance of human mitochondrial DNA. *Proc. Natl. Acad. Sci. USA.* 111:15474–15479. <https://doi.org/10.1073/pnas.1409328111>
- Ronneberger, O., P. Fischer, and T. Brox. 2015. U-Net: Convolutional Networks for Biomedical Image Segmentation. *Lect. Notes Comput. Sci.* 9351: 234–241. [https://doi.org/10.1007/978-3-319-24574-4\\_28](https://doi.org/10.1007/978-3-319-24574-4_28)
- Rørth, P.. 1998. Gal4 in the *Drosophila* female germline. *Mech. Dev.* 78:113–118. [https://doi.org/10.1016/S0925-4773\(98\)00157-9](https://doi.org/10.1016/S0925-4773(98)00157-9)
- Ross, J.M.. 2011. Visualization of mitochondrial respiratory function using cytochrome c oxidase/succinate dehydrogenase (COX/SDH) double-labeling histochemistry. *J. Vis. Exp.* (37). e3266.
- Satoh, M., and T. Kuroiwa. 1991. Organization of multiple nucleoids and DNA molecules in mitochondria of a human cell. *Exp. Cell Res.* 196:137–140. [https://doi.org/10.1016/0014-4827\(91\)90467-9](https://doi.org/10.1016/0014-4827(91)90467-9)
- Scaduto, R.C., Jr., and L.W. Grotyohann. 1999. Measurement of mitochondrial membrane potential using fluorescent rhodamine derivatives. *Biophys. J.* 76:469–477. [https://doi.org/10.1016/S0006-3495\(99\)77214-0](https://doi.org/10.1016/S0006-3495(99)77214-0)
- Shigenobu, S., K. Arita, Y. Kitadate, C. Noda, and S. Kobayashi. 2006. Isolation of germline cells from *Drosophila* embryos by flow cytometry. *Dev. Growth Differ.* 48:49–57. <https://doi.org/10.1111/j.1440-169X.2006.00845.x>
- Song, X., G.B. Call, D. Kirilly, and T. Xie. 2007. Notch signaling controls germline stem cell niche formation in the *Drosophila* ovary. *Development.* 134:1071–1080. <https://doi.org/10.1242/dev.003392>
- Spradling, A.C. 1993. Developmental Genetics of Oogenesis. In Bate M, editor. *The Development of Drosophila melanogaster*. Cold Spring Harbor, NY: Cold Spring Harbor Laboratory Press. pp. 1–70.
- Stephan, T., A. Roesch, D. Riedel, and S. Jakobs. 2019. Live-cell STED nanoscopy of mitochondrial cristae. *Sci. Rep.* 9:12419. <https://doi.org/10.1038/s41598-019-48838-2>
- Stewart, J.B., and N.G. Larsson. 2014. Keeping mtDNA in shape between generations. *PLoS Genet.* 10: e1004670. <https://doi.org/10.1371/journal.pgen.1004670>
- Stewart, J.B., C. Freyer, J.L. Elson, and N.G. Larsson. 2008a. Purifying selection of mtDNA and its implications for understanding evolution and mitochondrial disease. *Nat. Rev. Genet.* 9:657–662. <https://doi.org/10.1038/nrg2396>
- Stewart, J.B., C. Freyer, J.L. Elson, A. Wredenberg, Z. Cansu, A. Trifunovic, and N.G. Larsson. 2008b. Strong purifying selection in transmission of mammalian mitochondrial DNA. *PLoS Biol.* 6:e10. <https://doi.org/10.1371/journal.pbio.0060010>
- Stojanovski, D., O.S. Koutsopoulos, K. Okamoto, and M.T. Ryan. 2004. Levels of human Fis1 at the mitochondrial outer membrane regulate mitochondrial morphology. *J. Cell Sci.* 117:1201–1210. <https://doi.org/10.1242/jcs.01058>
- Taylor, R.W., and D.M. Turnbull. 2005. Mitochondrial DNA mutations in human disease. *Nat. Rev. Genet.* 6:389–402. <https://doi.org/10.1038/nrg1606>
- Trcek, T., T. Lionnet, H. Shroff, and R. Lehmann. 2017. mRNA quantification using single-molecule FISH in *Drosophila* embryos. *Nat. Protoc.* 12: 1326–1348. <https://doi.org/10.1038/nprot.2017.030>
- Tworzydło, W., E. Kisiel, W. Jankowska, A. Witwicka, and S.M. Bilinski. 2016. Exclusion of dysfunctional mitochondria from Balbiani body during early oogenesis of *Thermobia*. *Cell Tissue Res.* 366:191–201. <https://doi.org/10.1007/s00441-016-2414-x>
- Wallace, D.C.. 2005. A mitochondrial paradigm of metabolic and degenerative diseases, aging, and cancer: a dawn for evolutionary medicine. *Annu. Rev. Genet.* 39:359–407. <https://doi.org/10.1146/annurev.genet.39.110304.095751>
- Wallace, D.C., and D. Chalkia. 2013. Mitochondrial DNA genetics and the heteroplasmy conundrum in evolution and disease. *Cold Spring Harb. Perspect. Biol.* 5: a021220. <https://doi.org/10.1101/cshperspect.a021220>
- Wang, Z.H., Y. Liu, V. Chaitankar, M. Pirooznia, and H. Xu. 2019. Electron transport chain biogenesis activated by a JNK-insulin-Myc relay primes

- mitochondrial inheritance in *Drosophila*. *eLife*. 8. e49309. <https://doi.org/10.7554/eLife.49309>
- Werren, J.H., L. Baldo, and M.E. Clark. 2008. Wolbachia: master manipulators of invertebrate biology. *Nat. Rev. Microbiol.* 6:741-751. <https://doi.org/10.1038/nrmicro1969>
- White, P.M., L.R. Serbus, A. Debec, A. Codina, W. Bray, A. Guichet, R.S. Locke, and W. Sullivan. 2017. Reliance of *Wolbachia* on High Rates of Host Proteolysis Revealed by a Genome-Wide RNAi Screen of *Drosophila* Cells. *Genetics*. 205:1473-1488. <https://doi.org/10.1534/genetics.116.198903>
- Williams, C.C., C.H. Jan, and J.S. Weissman. 2014. Targeting and plasticity of mitochondrial proteins revealed by proximity-specific ribosome profiling. *Science*. 346:748-751. <https://doi.org/10.1126/science.1257522>
- Williamson, A., and R. Lehmann. 1996. Germ cell development in *Drosophila*. *Annu. Rev. Cell Dev. Biol.* 12:365-391. <https://doi.org/10.1146/annurev.cellbio.12.1.365>
- Zhang, Y., Y. Chen, M. Gucek, and H. Xu. 2016. The mitochondrial outer membrane protein MDI promotes local protein synthesis and mtDNA replication. *EMBO J.* 35:1045-1057. <https://doi.org/10.15252/embj.201592994>
- Zhang, Y., Z.H. Wang, Y. Liu, Y. Chen, N. Sun, M. Gucek, F. Zhang, and H. Xu. 2019. PINK1 Inhibits Local Protein Synthesis to Limit Transmission of Deleterious Mitochondrial DNA Mutations. *Mol. Cell*. 73:1127-1137.
- Zhou, R.R., B. Wang, J. Wang, H. Schatten, and Y.Z. Zhang. 2010. Is the mitochondrial cloud the selection machinery for preferentially transmitting wild-type mtDNA between generations? Rewinding Müller's ratchet efficiently. *Curr. Genet.* 56:101-107. <https://doi.org/10.1007/s00294-010-0291-5>

## Supplemental material

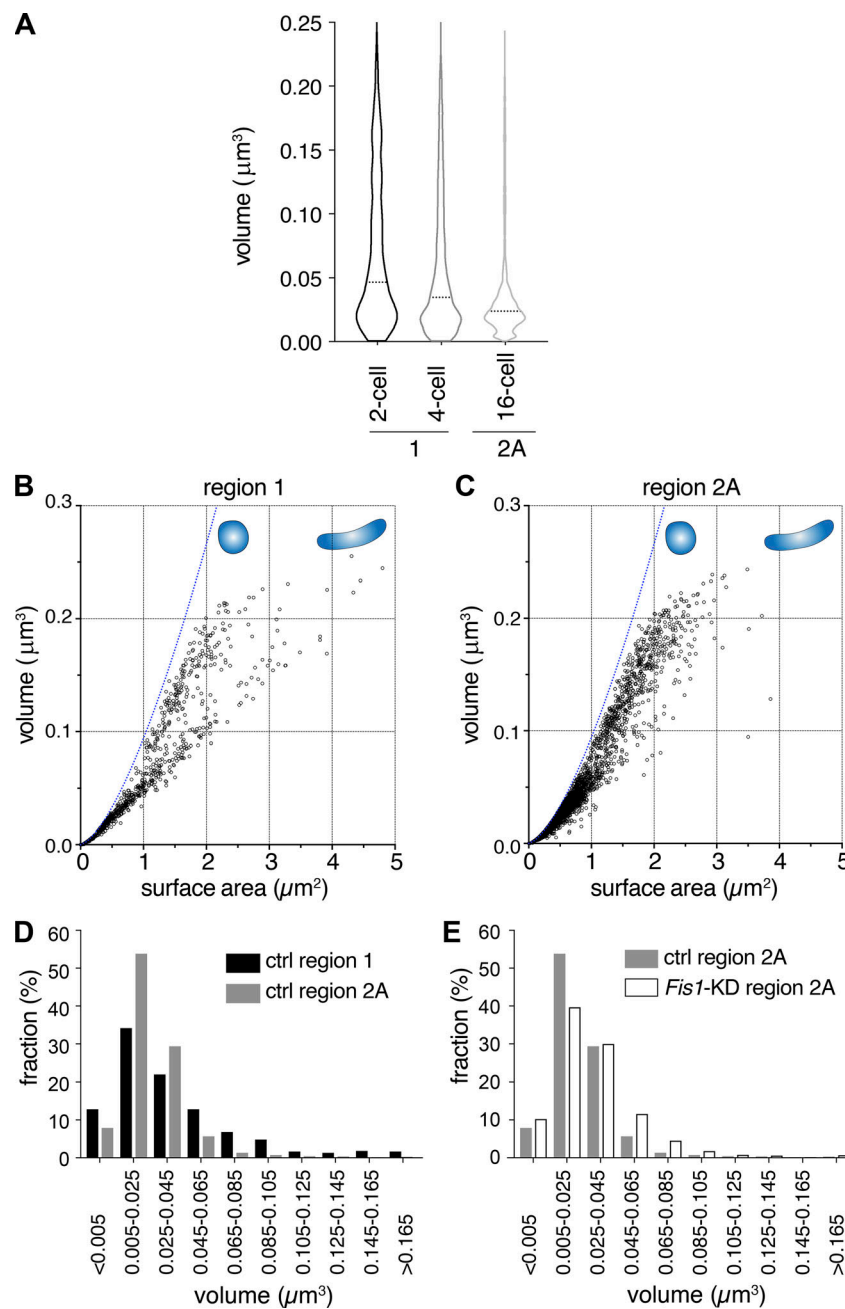


Figure S1. **FIB-SEM analyses show the change of mitochondrial volume and morphology in early germarium.** **(A)** A violin plot showing the distribution of individual mitochondrial volume in germarium 2-cell ( $n = 808$ ), 4-cell ( $n = 2,992$ ) and 16-cell ( $n = 4,782$ ) cysts. The dashed lines indicate the median volume. **(B and C)** The volume ( $V$ ) versus surface area ( $SA$ ) of each mitochondrion from regions 1 **(B)** and 2A **(C)** in wild-type ovaries. The dashed blue lines represent the relationship between  $V$  and  $SA$  of perfect spheres, which have the lowest  $SA/V$  ratio among all shapes. For a given volume, the lower  $SA/V$  reflects more rounded shape. Note that more mitochondria in region 2A shift toward the blue line, compared with those in 2-cell cyst at region 1. **(D and E)** Frequency distribution of mitochondrial volume in region 1 ( $n = 600$ ) and region 2A ( $n = 3,949$ ) of wild-type germarium **(D)**, and those in region 2A of wild-type and *Fis1* knockdown germarium ( $n = 3,509$ ; **E**). The mean voxel intensity was applied to filter out the light-stained objects, and only the densely stained objects were included in the analyses.



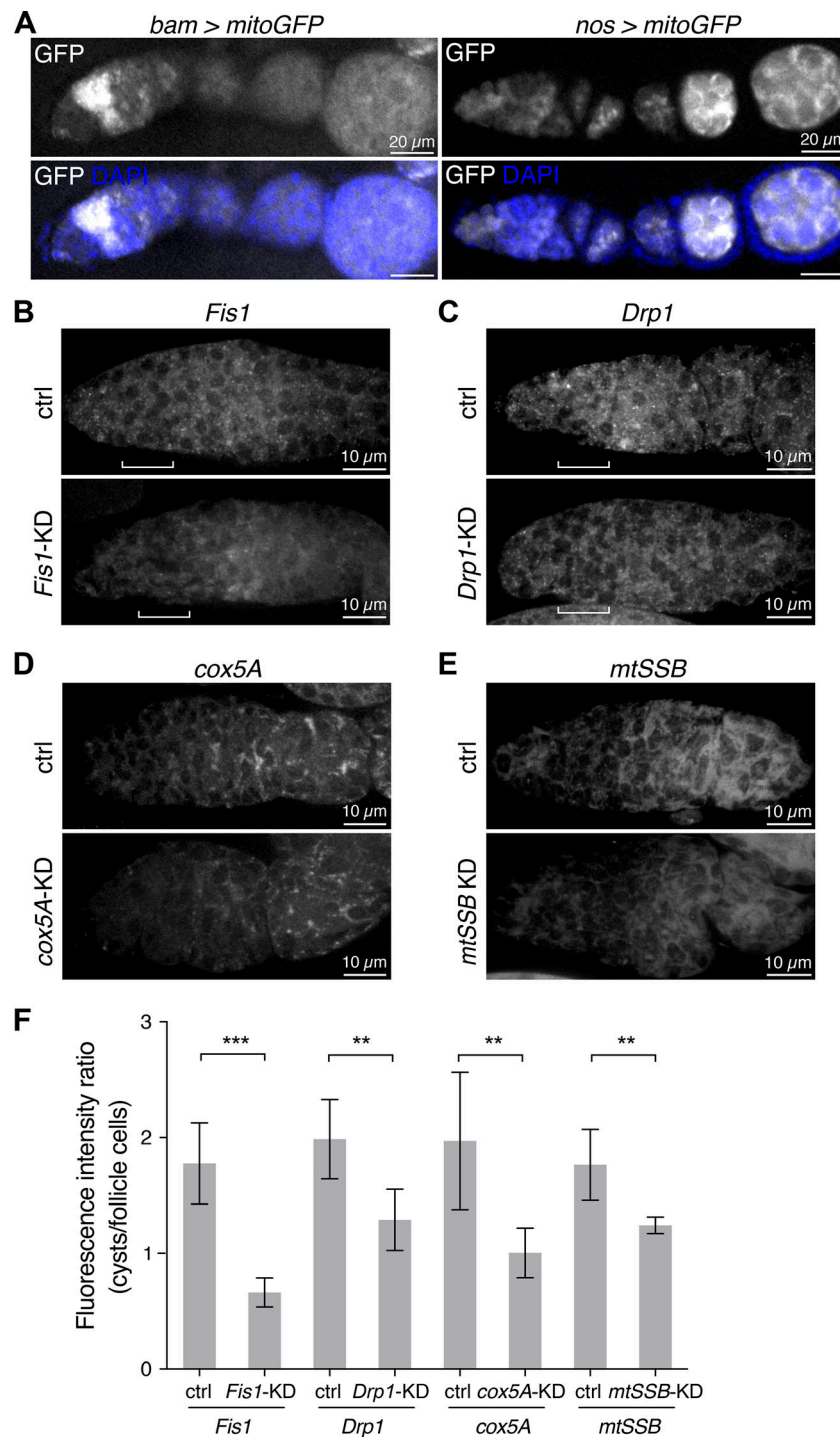


Figure S2. **Expression pattern of germline-specific drivers and FISH assay.** (A) Expression pattern of mitochondrially targeted GFP (mitoGFP) driven by *bam-gal4* and *nanos-gal4* drivers. Note the high expression level of mitoGFP in dividing cysts driven by *bam-gal4*. Ovaries are costained with DAPI (blue). Scale bar, 20  $\mu$ m. (B–E) smFISH assay showing the knockdown efficiency of several RNAi lines. The images are representative images of smFISH using DNA probes targeted to *Fis1* (B), *Drp1* (C), *cox5A* (D), and *mtSSB* (E) in ovaries. Brackets in B and C indicate region 2A. Scale bar, 10  $\mu$ m. (F) Quantification of the smFISH fluorescence intensity in germline cysts using region 2B follicle cells in the same germarium as the internal control ( $n = 4$  for each genotype). The ratio of the fluorescence intensity in germline cysts to follicle cells are shown. Data presented are means  $\pm$  SD. \*\*,  $P < 0.05$ ; \*\*\*,  $P < 0.001$ .

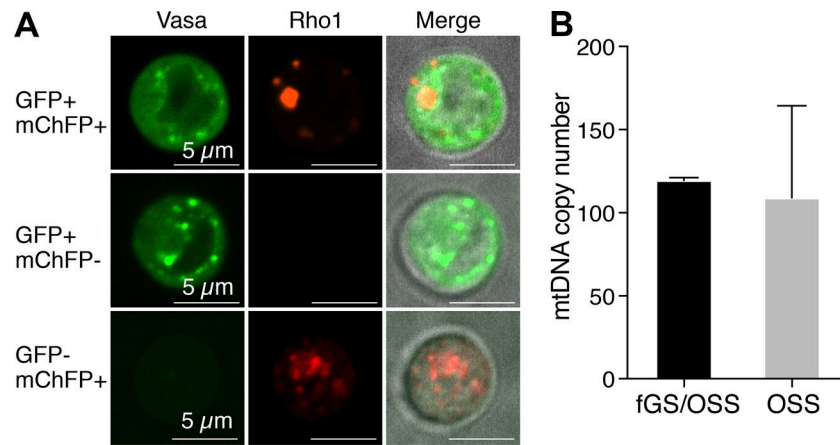


Figure S3. **Quantification of mtDNA copy number in GSCs.** (A) Confocal images of cells isolated from early pupae produced by crossing X/X; Vasa-GFP female flies with Rho1-mChFP/Y male flies using FACS. The female germ cells express both GFP and mChFP (Rho1-mChFP/X; Vasa-GFP/+), while male germ cells only express GFP (X/Y; Vasa-GFP/+). Somatic cells will not express GFP. The merged images are overlays of GFP, mChFP, and DIC channel. Scale bar, 5  $\mu$ m. (B) mtDNA copy number per cell in fGS/OSS (the mixture of fGSs and OSSs,  $n = 3$ ) and OSS ( $n = 5$ ) quantified by real-time PCR. The average copy numbers of mtDNA in fGS/OSS are 119.5 and 109, respectively. Thus, we deduced that the mtDNA number in fGS should be similar to that of fGS/OSS. Data presented are means  $\pm$  SD.

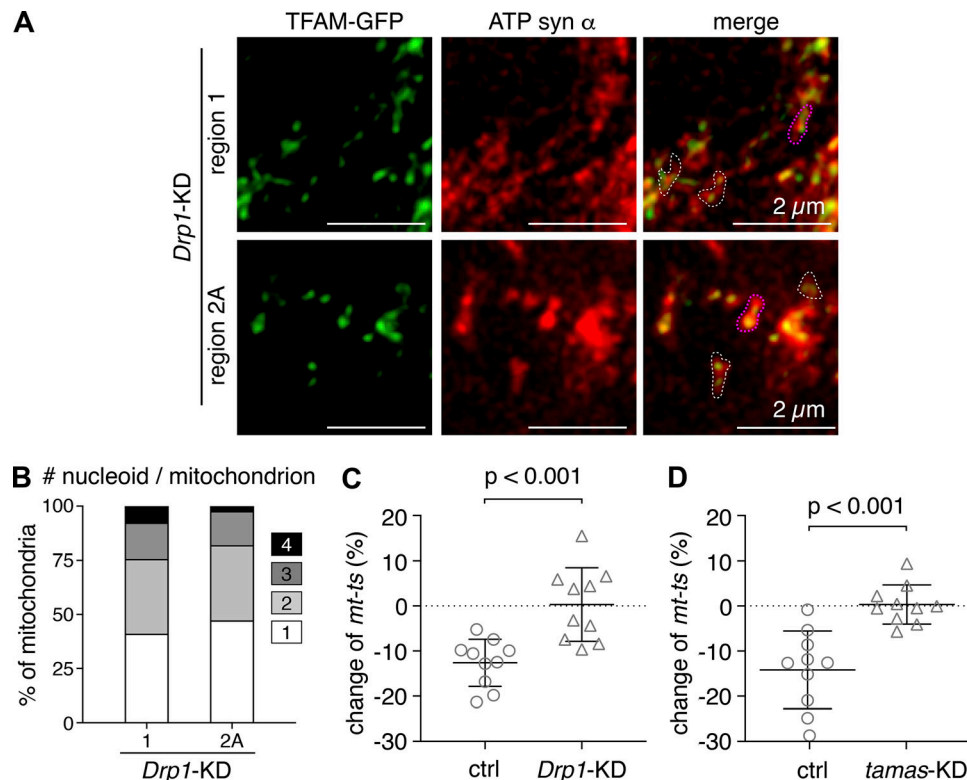


Figure S4. **mtDNA segregation and replication are required for selective inheritance.** (A) Representative images of the anterior end of regions 1 and 2A in a *Drp1* knockdown germarium (driven by *bam-gal4*) labeled with TFAM-GFP and ATPs. An object with continuous ATPs staining was defined as a single mitochondrion (white dashed lines). Two adjacent but distinct ATPs puncta were also called as a single mitochondrion if they appeared in the same contour and were connected with one nucleoid (magenta dashed lines). Scale bar, 2  $\mu$ m. (B) The number of nucleoids per mitochondrion was determined by counting the number of TFAM-GFP puncta within a single mitochondrion shown in A in regions 1 (GSCs or cystoblasts) and 2A from *Drp1* knockdown ovaries ( $n = 5$  germaria). The fraction of each group is shown. (C) Knockdown of *Drp1* using *bam-gal4* driver diminished the selection against the *ts* mtDNA in heteroplasmic *mt:Col<sup>T3001</sup> Dm* ( $n = 10$  for each genotype). Data presented are means  $\pm$  SD.  $P < 0.001$ . (D) Knockdown of *tamas* using *nanos-gal4* driver diminished the selection against the *ts* mtDNA in heteroplasmic *mt:Col<sup>T3001</sup> Dm* ( $n = 10$  for each genotype). Data presented are means  $\pm$  SD.  $P < 0.001$ .

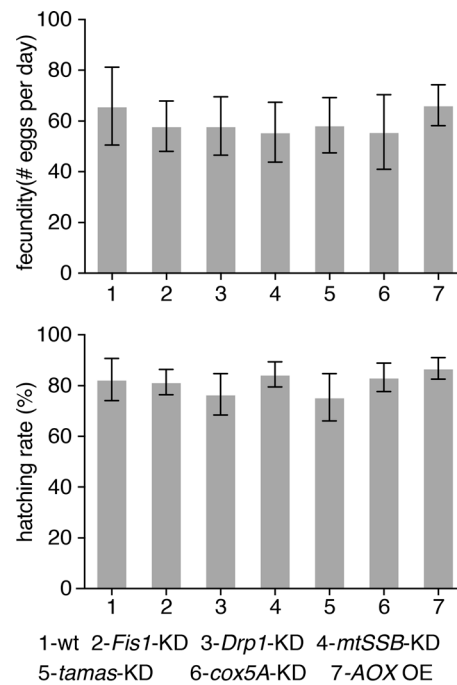


Figure S5. **Dm fecundity and hatching rate.** The fecundity and hatching rate of their progeny in *Fis1*, *Drp1* knockdown (driven by *bam-gal4*), *cox5A*, *mtSSB*, *tamas* knockdown (driven by *nanos-gal4*), and the AOX ectopic expression (driven by *nanos-gal4*) flies were comparable to those in wild-type flies. Fecundity,  $n = 15$  for wt, *cox5A*-KD, AOX OE;  $n = 11$  for *Fis1*-KD;  $n = 13$  for *Drp1*-KD;  $n = 14$  for *mtSSB*-KD;  $n = 12$  for *tamas*-KD. Hatching rate,  $n = 6$  for each genotype. Data presented are means  $\pm$  SD.

Video 1. **3D FIB-SEM image stack of wild-type *Dm* germarium with automated mitochondrial segmentation.** Y-stack images are shown, and time represents sequential images moving across the depth of the germarium (10-nm steps). Different cysts are decorated with different colors.

Video 2. **3D FIB-SEM image stack of *Fis1* knockdown germarium with automated mitochondrial segmentation.** Y-stack images are shown, and time represents sequential images moving across the depth of the germarium (10-nm steps). Different cysts are decorated with different colors.

Provided online are two supplemental tables. Table S1 shows the frequency (%) distribution of mitochondrial volume in control and *Fis1* knockdown (driven by *bam-gal4*) regions 1 and 2A. Table S2 shows the sequence of FISH short DNA probes targeting *ND4*, *Col*, *ND-SGDH*, *cox5A*, *Fis1*, *Drp1*, and *mtSSB*.